DNA topological regulation by topoisomerase IIβ-DNA-PK interaction is important for controlled hypoxia-inducible gene expression

Authors:

Heeyoun Bunch[1]*, Jihye Park[2], Min-Seok Seu[3], Jasmin K. Farmakes[4], Jeongho Lee[1], Ji-Seung Yoo[3], Huiming Lu[5], Young-Ran Yoon[6], Jae-Han Jeon[6], Matthew J. Schellenberg[4], Keunsoo Kang[2], Stuart K. Calderwood[7] and Anthony J. Davis[5]

Affiliations:

[1]Department of Applied Biosciences, Kyungpook National University, Daegu 41566, Republic of Korea

[2]Department of Microbiology, College of Bio-convergence, Dankook University, Cheonan 31116, Republic of Korea

[3]School of Life Sciences, BK21 FOUR KNU Creative Bioresearch Group, Kyungpook National University, Daegu 41566, Republic of Korea

[4]Department of Biochemistry and Molecular Biology, Mayo Clinic, Rochester, MN 55905, USA

[5]Department of Radiation Oncology, University of Texas Southwestern Medical Center, Dallas, TX 75390, USA

[6]School of Medicine, Kyungpook National University, Daegu 41944, Republic of Korea

[7]Department of Radiation Oncology, Beth Israel Deaconess Medical Center, Harvard Medical School, Boston 02115, USA

*Correspondence to HB at heeyounbunch@gmail.com

Present address:

S. K. Calderwood, The Hayden Rowe Writing Cooperative, Hopkinton, MA 01748, USA

M. Seu, Department of Chemistry, Ulsan National Institute of Science and Technology (UNIST), Ulsan 44919, Republic of Korea

ABSTRACT

Hypoxic stress responses are crucial for cellular and organismal survival and provoke gene regulation in diverse biological pathways including cell cycle progression and energy metabolism. Here, we

show that topoisomerase IIβ (TOP2B) regulates DNA topology and transcription in hypoxia-inducible genes (HIGs) in a DNA-PK-dependent manner. Cellular, mutational, and genomic analyses showed an antagonistic relationship between TOP2B and DNA-PK activities. TOP2B associates with HIGs and represses transcription by suppressing negative supercoiling formation under normoxic conditions. Under hypoxia, TOP2B is released, while DNA-PK and HIF1α are recruited to and activate HIGs. Intriguingly, DNA-PK is responsible for TOP2B to function repressively because DNA-PK knockout overturns both TOP2B release and activity and increases the expression of a number of HIGs. Mutational and genomic analyses confirmed that DNA-PK phosphorylates TOP2B at T1403 to stimulate TOP2B catalysis to suppress the open DNA conformation, which is important for controlled HIG transcription. Collectively, our findings suggest a novel role for TOP2B and DNA-PK-mediated TOP2B regulation as important transcriptional elements in HIG expression. We propose that TOP2B catalysis modulated by protein phosphorylation is coordinated with transcriptional states and determines DNA topology to regulate Pol II transcription.

Keywords:
Hypoxia-inducible genes; topoisomerase IIβ; DNA-PK; RNA polymerase II transcription; gene regulation; DNA topological regulation

INTRODUCTION

Transcription is the first step in gene expression. The process involves the polymerization of nascent RNA molecules catalyzed by enzymes called RNA polymerases. Their engagement, dissociation, and catalytic activity is tightly regulated by transcription factors and chromosome-associated elements[1]. In eukaryotic transcription, RNA polymerase II (Pol II) catalyzes the polymerization of mRNAs and most of the small- and long-noncoding RNAs, excluding rRNAs and tRNAs. Since the discovery of Pol II in 1969, extensive efforts have been made to advance our knowledge of the mechanisms of the Pol II gene regulation[2]. Such mechanisms, in a majority of genes, occur throughout the stages of transcription of initiation, early elongation, processive elongation, and termination, in response to the signals that activate or deactivate gene expression[3,4].

Gene regulation involves responses to cellular needs, extracellular signals, and the maintenance of homeostasis. Hypoxia is an acute stress that occurs when cells are deprived of oxygen supply[5].

Oxygen is the final molecule to receive protons in the mitochondrial electron transport chain[6]. These two atoms covalently bond to generate H_2O as a byproduct, resulting in the generation of an electrochemical gradient across the mitochondrial inner membrane. The gradient is the essential force for ATPase to synthesize ATP, the major organismal chemical energy source[6]. Therefore, the optimal concentration of O_2, required for efficient energy metabolism, is vital for cells to sustain, function, and grow[7,8]. Under the low concentration of oxygen imposed by the adverse conditions such as infection, inflammation, cardiovascular diseases, and cancer, cells need to cope with and survive hypoxic stress by increasing angiogenesis, glycolysis, and metastasis[9-12]. A number of genes in these hypoxia-stimulated pathways, called hypoxia-inducible genes (HIGs), are activated. The most well-known mechanism to regulate such gene activation involves HIF1α, a transcription factor, which is stabilized by the limited availability of O_2 in cells[5,13-16]. Stabilized HIF1α relocates into the nucleus and is dimerized with HIF1β. Heterodimeric HIF1α–HIF1β complex binds to the hypoxia-responsive elements in the promoters of its target genes and triggers transcriptional activation[8].

DNA-PK holoenzyme, a kinase complex, composed of a DNA-PK catalytic subunit (DNA-PK hereafter) and a Ku70/Ku80 heterodimer, is well-known for its role in the repair of DNA double-stranded breaks[17,18]. The protein functions as a central factor for DNA repair via nonhomologous end joining, although some studies also suggest its facilitating role in DNA repair via homologous recombination[18-20]. In our previous study, interestingly and unexpectedly, DNA-PK and one of its substrates, TRIM28, were identified to regulate the Pol II promoter-proximal pause (Pol II pausing, hereafter) release at *HSPA1B* (*HSP70*) and immediate early genes (IEGs), including *EGR1*, *JUN*, *FOS*, and *MYC*[21-24]. TRIM28 stabilizes Pol II pausing during the resting state of transcription, whereas upon the reception of activating signals, it is phosphorylated at S824 by DNA-PK and ATM, an event that contributes to Pol II pause release[21]. Interestingly, a recent study reported that DNA-PK and TRIM28 are important transcriptional activators involved in Pol II pausing and pause release of HIGs[25,26], similarly to the case of IEG activation[22,23]. In both studies, inhibiting DNA-PK catalytic activity, thus preventing the phosphorylation of its substrates and DNA damage response signaling, impeded gene activation, indicating a crucial role of DNA-PK as a transcriptional elongation factor for these genes.

Mammalian topoisomerase II (TOP2) is a DNA topology factor, whose torsion-relieving catalysis is required for effective DNA metabolism processes such as replication, transcription, and DNA compaction into nucleosomes[27,28]. Our own and others' recent studies indicate topoisomerase IIβ (TOP2B) recruitment near the transcription start site (TSS) and functional involvement in the transcriptional activation of estrogen- and androgen receptor genes, *HSP70*, neurotransmitter-inducible genes, retinoic acid responsive genes, and IEGs[22,29-36]. Although it is unclear whether the DNA strand break caused by TOP2B is programmed or accidental, the DNA break and damage response signaling caused by TOP2B catalytic activity stimulates the activation of these genes[22,35]. Importantly, the topological states of these genes before and during transcription activation remain to be elucidated. Although both positive and negative supercoiling in excess could hinder Pol II movement, some studies have indicated that negative supercoiling in the promoter, accumulated by Pol II forward translocation, favors transcription, whereas positive supercoiling ahead of elongating Pol II is rather inhibitory to the enzyme progression[37-42]. These observations propose the potential biphasic effects of TOP2B activities that the neutralization of negative supercoiling by TOP2B in that the promoter could suppress transcriptional activation, whereas relieving positive supercoiling in the downstream of Pol II may facilitate it. To note, the regulation of TOP2B binding, catalysis, and dissociation during gene activation is thought to occur through post-translational modifications. Our previous studies reported, for instance, that TOP2B ubiquitination by the BRCA1–BARD1 complex increases the affinity between TOP2B and the DNA and that TOP2B phosphorylation by ERK2 modulates TOP2B catalysis of positive and negative DNA supercoiling and TOP2B dissociation from the target gene[34,35].

Although TOP2B, as well as DNA-PK, is reportedly involved in the activation of estrogen- and androgen receptor genes, *HSP70*, neurotransmitter- and retinoic acid-inducible genes, and IEGs, and DNA-PK is reportedly important for hypoxic gene regulation[22,26,29,30,32-36], the potential role of TOP2B in HIG transcription has not been studied. Additionally, TOP2B physically interacts with XRCC6 (Ku70), while DNA-PK neither binds to nor is activated with the broken DNA end of the TOP2B-DNA adduct[43,44]. These findings suggest the intriguing possibility of cross-talk and regulation between TOP2B catalysis and DNA-PK activation in HIG transcription. In this study, we have examined whether TOP2B is involved in HIG transcription, whether TOP2B interacts with DNA-PK, and, if so, the role of their interaction. Our present data revealed for the first time that TOP2B suppresses HIG

transcription under normoxic conditions and is catalytically restricted and released from the HIG genes under hypoxic conditions. DNA-PK has biphasic effects on HIGs in that the DNA-PK knockout (KO) increases or decreases the expression of different subsets of HIGs. Intriguingly, DNA-PK modulates TOP2B towards repressive transcription and contributes to regulating TOP2B activity and release. In the absence of DNA-PK, TOP2B stimulates HIG transcription. Conversely, TOP2B interferes with DNA-PK and HIF1α recruitment and DNA-PK phosphorylation at T2609 and suppresses HIG transcription. Our mutational and genome-topological analyses suggest that DNA-PK phosphorylates TOP2B at the C-terminal domain (CTD), including residue T1403, a modification which apparently suppresses HIG transcription by removing negative supercoiling.

RESULTS

HIG expression is regulated by TOP2

DNA structure and topology have been recognized as important transcription regulatory elements of diverse stimulus-inducible metazoan genes[29,32,33,35,45-51]. In humans, the TOP1 and TOP2 enzymes resolve the negative and positive DNA supercoiling associated with DNA metabolism, including transcription[52]. In this study, we have investigated whether human TOP2 is involved in HIG transcriptional regulation. Representative HIGs, such as *p21*, *ALDOC*, *GLUT*s, and *IL1β*, were analyzed throughout the study[5,11,14,53-55]. $CoCl_2$, a chemical validated to mimic hypoxic conditions in multiple studies[12,56,57], was supplemented to cells at a final concentration of 200 μM for 12 h to induce hypoxic responses in human neuroblastoma cells, SH-SY5Y. The qRT-PCR results revealed significant transcriptional activation at *p21*, *ALDOC*, *IL1β*, and *GLUT1* under $CoCl_2$-mediated hypoxic stress (**Fig. 1A** and **Supplementary Figure 1A**). Under the same hypoxic conditions, using the ChIP-PCR analysis, it was shown that the master transcriptional activator for HIGs, HIF1α was recruited to the TSSs of these genes, whereas the level of TOP2B occupancies was notably decreased in the TSSs as well as the gene bodies (GBs) (**Fig. 1B** and **Supplementary Figure 1B**). Initially, TOP2A was rarely considered as a transcription factor, and thought as a DNA replication factor, until recent studies indicated that TOP2A also functions in transcription[58,59]. Therefore, TOP2A was monitored at the representative HIGs. Our data indicated a similar behavior of TOP2A to that of TOP2B in that both proteins dissociated from the promoters of the HIGs upon gene activation (**Fig. 1C**). It is noted that TOP2B has been generally known as a transcriptional activator and is recruited to stimulated

stress-inducible genes, including *HSP70*, IEGs, estrogen- and androgen activated genes, and neurotransmitter-inducible genes[22,23,29,32-35,60]. Therefore, the release of TOP2A and TOP2B from representative HIGs upon gene activation was an unprecedented and unexpected finding to our knowledge and suggested a distinctive regulatory mechanism involving TOP2B in HIG transcription.

To understand TOP2B–genome interaction under hypoxic conditions, we next investigated TOP2 engagement with chromosomal DNA using an ICE assay. $CoCl_2$-induced hypoxic conditions increased the levels of TOP2A and TOP2B associated with the genome (**Fig. 1D**). As expected, etoposide, a chemical inhibitor of both TOP2s that traps the proteins in the TOP2–DNA covalent cleavage complex (TOP2cc)[61], increased both TOP2A and TOP2B associated with the DNA under normoxic conditions. Interestingly, however, under hypoxic conditions, the etoposide-poisoned TOP2B protein was dramatically reduced (**Fig. 1D** and **Supplementary Fig. 1C**), indicating either a reduction in catalytically active TOP2B or a hyperactive TOP2cc removal pathway, or both. In our previous studies, we observed that etoposide activates, whereas ICRF193, a catalytic inhibitor of TOP2, represses the transcription of IEGs, such as *EGR1* and *FOS*[22,35]. Therefore, each of these two TOP2 inhibitors at 10 μM as a final concentration, along with 200 μM $CoCl_2$, was applied to SH-SY5Y cells for 3 h, and the cells were analyzed using qRT-PCR. The data illustrated that both etoposide and ICRF193 upregulated the mRNA levels of representative HIGs (**Fig. 1E**), suggesting that the catalytic activity of TOP2 inhibits productive transcription. Overall, the data in **Fig. 1** indicated a novel, suppressive role for TOP2 in regulating the transcription of HIGs through some unique mechanisms.

HIG expression is regulated by the TOP2B–DNA-PK interaction

As mentioned earlier, a recent study reported the important role of DNA-PK in HIG transcription[26], and one of the functional subunits of the DNA-PK holoenzyme, XRCC6 (Ku70) physically interacts with TOP2[43]. Therefore, we examined whether TOP2B could also interact with DNA-PK. Immunoprecipitation against HeLa nuclear extracts was performed. To ensure that only stable protein interactions were identified, immunoprecipitation with stringent washes using 0.15–0.5 M HEGN with >130-fold bead volume was performed, followed by immunoblotting. The data showed that TOP2B pulled down DNA-PK, and vice versa (**Fig. 2A**), indicating their stable, strong physical interaction. As previously reported[26], HIF1α was found to interact with DNA-PK in our assays. On the other hand, HIF1α did not interact with TOP2B (**Fig. 2A**).

Next, we aimed to understand the role of the interaction between TOP2B and DNA-PK in HIG transcription. DNA-PK-KO HCT116 cells, which were generated and characterized in a previous study[62,63], were used, and the KO was validated by immunoblotting (**Fig. 2B**). We did not observe a notable reduction in the TOP2B protein levels despite attenuated smeared upper band formation, potentially representing posttranslationally modified TOP2B, in DNA-PK KO cells (**Fig. 2B**). Similarly, the γH2AX level was rarely affected by DNA-PK KO (**Fig. 2B**). We found that the absence of DNA-PK dramatically hindered HIF1α stabilization under $CoCl_2$-induced hypoxic conditions (**Fig. 2C**), indicating an important role for DNA-PK in HIF1α-mediated hypoxic responses in cells. TOP2B occupancies at representative HIGs were monitored and compared in the presence and absence of DNA-PK, using ChIP-qPCR analyses. Strikingly, DNA-PK KO increased TOP2B occupancies under normoxic conditions in all three HIGs tested, *p21*, *ALDOC*, and *IL1β* (**Fig. 2D**). Importantly, TOP2B dissociation under hypoxic conditions was reversed, rather further increasing TOP2B, in the absence of DNA-PK (**Fig. 2D**). These results suggested that DNA-PK causes TOP2B to be repressive for transcription, and thus, in the absence of DNA-PK, TOP2B apparently contributes to HIG transcriptional activation. Supporting this speculation, DNA-PK KO or catalytic mutant DNA-PK with K3753R mutation[63] resulted in significantly increased mRNA production at representative HIGs (**Fig. 2E** and **Supplementary Figure 2A**).

The upregulated transcription without functional DNA-PK, in spite of compromised HIF1α stabilization in DNA-PK KO cells, (**Figs. 2C–E**) was unexpected and rather perplexing. Therefore, we performed RNA-seq to compare WT and DNA-PK KO cells with or without $CoCl_2$-induced hypoxic stress (200 μM $CoCl_2$ supplemented for 12 h). The results demonstrated that a total of 258 genes [$|Log_2$Fold change (FC)| > 0.5, $p < 0.05$] were increased (n = 192) or decreased (n = 66) in mRNA expression (**Fig. 3A** and **Supplementary Data 1**). Importantly, DNA-PK KO affected a large number of genes (n = 4700, **Fig. 3B** and **Supplementary Data 2**), and approximately 58% of the differentially expressed genes (n = 2706) were upregulated in the absence of DNA-PK (**Fig. 3B** and **Supplementary Data 2)**. Among hypoxia-induced genes, 40.6% genes (n = 78) were differentially expressed in DNA-PK KO cells, and most of those (88.5%) showed increased expression levels without DNA-PK (**Fig. 3C** and **Supplementary Data 1,2**), suggesting a repressive role of DNA-PK in HIG transcription. We examined individual HIGs, extensively studied for their functions in hypoxic responses, and presented

some of them (|FC| > 0.5, p-value < 0.05) that displayed distinctive expression patterns in the presence or absence of DNA-PK (**Fig. 3D**). *MMP25*[64] and *HK2*[65] were among approximately 11.5% downregulated genes, whereas more genes, including *ANKRD37*[66], *DDIT4*[67], *p21*, *ALDOC*, and *GLUT3*, showed increased gene expression without DNA-PK (**Fig. 3D**).

We also examined TOP2B occupancies in HIGs using the previous TOP2B ChIP-seq data (GSM2442946, **Supplementary Data 3**). Seventy-six percent of the 192 HIGs identified (n = 146) were occupied by TOP2B (**Fig. 3E**, red dots). Among the genes downregulated under hypoxic conditions, approximately 42% genes were bound by TOP2B (**Fig. 3E**, blue dots). Overall, >67% of hypoxia-regulated genes, either upregulated or downregulated, were occupied by TOP2B, indicating an important role for this protein in hypoxic responses. Additionally, TOP2B occupancy in DNA-PK-regulated genes was analyzed. The data illustrated that about 54% of the genes upregulated (n = 1455, red dots) and 48% of the genes downregulated (n = 957, blue dots) by DNA-PK KO, respectively, were occupied by TOP2B (**Fig. 3F**), indicating DNA-PK and TOP2B functional interactions in a large number of genes in humans. GO analyses of DNA-PK KO-increased genes occupied by TOP2B revealed that these genes are involved mainly in the pathways to control cellular morphogenesis and mobility (**Supplementary Figure 3A** and **Supplementary Data 4**), suggesting a suppressive role of DNA-PK and DNA-PK-TOP2B interactions on these genes. On the other hand, GO analyses of DNA-PK KO-decreased genes occupied by TOP2B showed that they are involved in ribonucleoprotein complex biogenesis, transcription, and DNA metabolism (**Supplementary Figure 3B** and **Supplementary Data 4**), suggesting the activating role of DNA-PK and DNA-PK-TOP2B interactions in these pathways. Overall, these data that are presented in **Fig. 3** suggested a DNA-PK-dependent suppressive role of TOP2B in HIG transcription and the TOP2B–DNA-PK interaction for transcriptional regulation of a number of genes including HIGs.

TOP2B regulates HIF1α and DNA-PK recruitment and activity in HIGs

Our data showed that, under hypoxic stresses, TOP2B was released from representative HIGs in WT cells, whereas it was recruited to these genes in DNA-PK KO cells (**Figs. 1A,B,2D,E**), indicating that DNA-PK modulates TOP2B behavior and function. To understand the relationship further, we monitored DNA-PK in TOP2B KO SH-SY5Y cells[36]. TOP2B KO was confirmed through immunoblotting (**Fig. 4A**). In TOP2B KO cells, total cellular DNA-PK protein levels were not

noticeably affected (**Fig. 4A**). Cells were treated with 200 μM $CoCl_2$ or H_2O (–$CoCl_2$, control) for 6 h, and ChIP-qPCR was performed. As previously reported, DNA-PK was modestly recruited under hypoxic stress in WT cells at the representative HIGs (**Fig. 4B**). Interestingly, DNA-PK occupancy was significantly increased in TOP2B KO cells under normoxic conditions and maintained to the similar levels under hypoxic conditions (**Fig. 4B**).

Next, levels of phosphorylated DNA-PK at T2609 (pDNA-PK) were monitored because this site is known to be phosphorylated by ATM and/or by itself and is a signature modification of activated DNA-PK[22]. In WT cells, pDNA-PK levels were increased under hypoxic stress (**Fig. 4C**). Importantly, consistent with the increased DNA-PK levels, pDNA-PK occupancy was significantly increased in TOP2B KO cells even under normoxic conditions compared with WT (**Fig. 4C**). For DNA-PK–HIF1α interaction (**Fig. 2A**), HIF1α occupancy in the promoters of the representative HIGs was also monitored. As expected, HIF1α was recruited to the genes under hypoxic stress in WT cells (**Fig. 4D**). In a similar manner to that of DNA-PK and pDNA-PK, HIF1α occupancies were significantly increased under normoxic conditions in TOP2B KO cells (**Fig. 4B–D**). Consistent with the recruitment of DNA-PK, pDNA-PK and HIF1α, the transcription of the representative HIGs, except for *p21*, was already activated in normoxic conditions and then further activated in the hypoxic conditions in the absence of TOP2B (**Fig. 4E**). Together, the data presented in **Fig. 4** suggested that TOP2B functions to prevent DNA-PK and HIF1α from associating with HIG genes and DNA-PK phosphorylation at T2609 and suppresses transcription.

TOP2B phosphorylation by DNA-PK is repressive for HIG transcription

Because TOP2B interacts with DNA-PK physically and functionally (**Figs. 2A,3F,4B,C**), we asked whether DNA-PK phosphorylates TOP2B. Through phosphopeptide mass spectrometry, WT, DNA-PK KO, and the KO cells overexpressing the catalytically null DNA-PK mutant (K3753R) were compared to identify six TOP2B peptides that included residues phosphorylated by DNA-PK (phosphorylation sites identified in H. Lu and A.J. Davis manuscript in preparation). The sites encompassing these six peptides were selected for further analyses (**Fig. 5A**). All six peptides were located in the carboxy-terminal domain (CTD) of TOP2B. As we focused particularly on TOP2B in HIG transcription, the phosphorylatable residues within the six peptides, which are unique to TOP2B sequences and yet distinctive from those of TOP2A sequences, were screened via primary sequence

comparisons. The TOP2B-unique sequences are underlined, and the five phosphorylatable sites are marked in red (numbering using TOP2B longest isoform 1; **Fig. 5A**). To understand the function of DNA-PK-mediated TOP2B phosphorylation, these sites were individually mutated into alanine (A), and the WT and resultant TOP2B mutants were expressed in TOP2B KO SH-SY5Y cells. Although TOP2B variants were difficult to overexpress because of reportedly low transfection efficiencies of this cell line, their modest expression levels were confirmed by immunoblotting (**Fig. 5B**).

WT and the five mutant TOP2B-expressing cells were analyzed for the mRNA levels using qRT-PCR. Among these mutants, T1403A TOP2B exhibited consistently increased transcription of the representative HIGs, *p21*, *ALDOC*, and *IL1β*. At another site, the S1526A mutation decreased mRNA levels for *p21* and *ALDOC* but increased the *IL1β* mRNA level (**Fig. 5C**). These TOP2B mutants were compared with the WT under hypoxic conditions. Cells were supplemented with $CoCl_2$ at 200 μM for 12 h at 48 h post-transfection, and the mRNA expression of representative HIGs was quantified using qRT-PCR. Consistent with the data obtained under normoxic conditions, T1403A increased the mRNA production of all three tested genes (**Fig. 5D**), suggesting that T1403 phosphorylation by DNA-PK may cause TOP2B to be repressive for transcription in HIGs. For S1526A, mixed expression patterns were observed for these genes (**Fig. 5D**).

TOP2B restricts "DNA openness" to prevent HIG activation under normoxia

To understand the mechanism of DNA-PK-mediated TOP2B regulation, we utilized trimethylpsoralen–sequencing (TMP–seq). TMP is a small organic chemical that can be intercalating into negatively supercoiled DNA and the TMP-DNA complex can be cross-linked by UV light. The genomic regions incorporated by TMP were collected through removing TMP-free regions by chromatin fragmentation and repeated DNA denaturation and digestion using DNases (**Fig. 6A**). Then topological changes in WT and TOP2B KO SH-SY5Y cells were monitored and compared. Our metagene analyses showed that genomic regions (n = 60649 genes; –1 Kb from TSS to +1 Kb from transcription end site [TES]) were markedly underwound in TOP2B KO cells, compared with WT cells (Left panels, **Fig. 6B**). Open DNA regions around TSSs (n = 60649 genes; –0.5 Kb to +1 Kb from TSS) were more detectable in TOP2B KO cells than WT cells (heatmaps on the right panels, **Fig. 6B**). DNA topologies on the genes that were identified as hypoxia-induced (n = 192) or -repressed (n = 66) by RNA-seq (**Figs. 3A,C,E**) were monitored and compared under normoxia and hypoxia (**Fig.**

6C–E and **Supplementary Figures 4A,B**). Strikingly, DNA around approximately +200 regions became markedly negatively-supercoiled or underwound under hypoxia-inducible gene activation (marked with a red asterisk; **Fig. 6C**). On the other hand, this spike of open DNA topology formation under hypoxic conditions was not observed in TOP2B KO cells, although DNA were overall more open near the TSS under normoxia (marked with yellow tint; **Fig. 6D**). A chromosome view of *ALDOC* genomic region depicted increased DNA negative supercoiling in the TSS under normoxic conditions in TOP2B KO, compared to the WT (marked with a green box; **Fig. 6E**).

Metagene analyses of total genes (n = 60649) showed the architecture of genome, in which the GB regions were overall less open than promoters or beyond TES under normoxia (–hypoxia; left panel; **Fig. 6F**). Interestingly, the genome appeared to be more open throughout the promoter, TSS, GB, and TES under hypoxia (+hypoxia; left panel; **Fig. 6F**). In contrast, TOP2B KO caused the genomic DNA to be much more open than that in the WT under normoxia (–hypoxia; right panel; **Fig. 6F**), whereas the DNA was not further unwound under hypoxia without TOP2B (+hypoxia; right panel; **Fig. 6F**).

To understand the role of DNA-PK-mediated TOP2B phosphorylation in genomic DNA topology, the WT TOP2B and the TOP2B T1403A mutant, which showed a consistent increase in the transcription of representative HIGs (**Fig. 5**), were expressed in TOP2B KO cells, and the underwound DNA regions under hypoxia were mapped through TMP–seq. It was notable that a valley, presumably more tightly wound DNA regions, at the approximately +600 almost disappeared in T1403A TOP2B cells (left panel, **Fig. 6G**), suggesting that TOP2B phosphorylation at T1403 by DNA-PK might be responsible for relaxing the negative supercoiling in the downstream of TSSs. GB and TES also accumulated more open DNA structures in T1403A TOP2B cells, compared to WT cells (middle and right panels, **Fig. 6G**). These open DNA signatures were consistent with more active transcription of representative HIGs in TOP2B T1403A and DNA-PK KO cells (**Figs. 2D,E,3D,5C,D**), suggesting that DNA-PK-mediated phosphorylation of TOP2B at T1403 enables controlled transcription by suppressing negative supercoiling/underwound DNA formation in HIGs.

DISCUSSION

In this study, we identified TOP2B as a novel factor to regulate human HIG transcription, and found that TOP2B dynamically interacts with DNA-PK. These molecules appear to regulate the activities of each other and thus controls HIG transcription. Because we have been regarding TOP2B as a transcriptional activator for many genes including *HSP70*, IEGs, androgen/estrogen receptor genes, and neuronal activity-inducible genes in our and others' previous studies[21,22,24,29,32-35], the finding from this study that TOP2B suppresses HIG transcription was rather surprising and intriguing. In addition, our mutational and RNA-seq analyses suggest that DNA-PK plays dual roles on HIG transcription, as an activator for some and a repressor for other HIGs (**Fig. 3** and **Supplementary Figure 3** and **Supplementary Data 1,2**), rather than an activator for all HIGs as previously reported[26]. Our data support the concept that DNA-PK is important for HIF1α recruitment as reported by the above study[26] (**Fig. 2A**) and suggest that DNA-PK KO devastates HIF1α stabilization under hypoxia (**Fig. 2C**). Interestingly, however, HIG transcription is still robust without DNA-PK and HIF1α recruitment in DNA-PK KO cells (**Figs. 2E,3D** and **Supplementary Figure 2**). This may be explained by a dependence on or a transition to HIF2 in HIF1 instability[68,69], and that DNA-PK has a suppressive role in the transcription of many HIGs through its interaction with TOP2B.

Our data suggest that TOP2B is associated with HIGs and prevents DNA-PK and HIF1α from being recruited under normoxia (**Figs. 4B–D**). DNA-PK recruitment under hypoxia is likely to be important for TOP2B release from the HIGs as DNA-PK KO overturns TOP2B release (**Fig. 2D** and **Supplementary Figure 2**). DNA-PK presence also controls the ability of TOP2B activity to be suppressive because, without DNA-PK, TOP2B stimulates HIG transcription without being released under hypoxia and even under normoxia (**Figs. 2D,E,3D**). An unphosphorylatable mutant TOP2B, T1403A and genomic topology studies suggest that TOP2B removes negative supercoiling formation to suppress HIG transcription, and DNA-PK phosphorylation stimulates TOP2B catalysis to relax the negative supercoiling (**Figs. 5C,D,6B–G**). It is notable that normal hypoxic responses release TOP2B (**Fig. 1**) and involve a dramatic increase in negative supercoiling or DNA underwinding in the TSSs of HIGs, which was only observed in the WT, not in TOP2B KO cells (**Figs. 6C,D**). These observations in HIG transcription may be in agreement with a previous study showing that transcriptionally-active regions in the genome are overall underwound and tend to be devoid of TOP2[70].

In HIGs, TOP2 seems to take a more active and important role under normoxia (**Figs. 1B–E,2D,E** and **Supplementary Figure 1C**) to maintain the resting state of HIG expression. In our model (**Fig. 7**), we propose that TOP2B relaxes negative DNA supercoiling to prevent it from accumulating in the TSS and also interferes with DNA-PK and HIF1α recruitment to the promoter of HIGs under normoxia. Under hypoxia, DNA-PK recruitment and activation, along with HIF1α, presumably mediates TOP2B release and activates transcription. Our current data suggest that DNA-PK phosphorylates TOP2B at T1403 to stimulate TOP2B catalytic activity and resolve negative supercoiling under normoxia. It is unclear how TOP2B is released from HIGs and what the exact function of DNA-PK, except for augmenting HIF1α recruitment, is under hypoxia, an activity which awaits further investigations. It is particularly of interest to ask whether the role of DNA-PK involves DNA repair or some other aspect of HIG activation. DNA-PK appears to switch functions depending on the DNA structures that it associates with. In a recent study, for example, identified that binding to the open DNA ends, DNA-PK suppresses autophosphorylation at T2609 but phosphorylates other protein targets[71]. Another previous study reported unique phenomena, particularly that TOP2B is recruited to the loci of DNA double strand breaks[72]. It is possible that DNA break causes underwound DNA and topological stresses, requiring TOP2B to restore the superhelicity. Also, it is plausible that TOP2B recognizes the broken ends after DNA break as intermediate (transition state) substrates as TOP2B binds to twisted DNA, induces DNA break, and joins the DNA ends, suggesting that TOP2B binds to both intact and broken DNA ends. In the case of the latter, KU proteins and DNA-PK may substitute TOP2B on the lesion upon the release of TOP2B in HIG activation. The resolution of these conjectures and the molecular events with detailed mechanisms including the local DNA structures, in which TOP2B and DNA-PK are associated with, will be a goal for future studies.

Our previous study showed that TOP2B ubiquitination by the BRCA1-BARD1 complex is important for TOP2B-*EGR1* TSS interaction during transcriptional rest. Upon transcriptional activation, the phosphorylation of BRCA1 at S1524 by ATM/ATR discouraged the BRCA1-BARD1-mediated TOP2B ubiquitination to lower the affinity between TOP2B and *EGR1* DNA[34]. In addition, ERK2 phosphorylates the CTD of TOP2B and regulates its catalytic activity to resolve the positive DNA supercoiling[35]. On the other hand, ERK2 delays the TOP2B catalysis of relaxing the negative DNA supercoiling[35]. In this study, DNA-PK phosphorylates the CTD of TOP2B to augment the catalysis of negative DNA supercoiling, an event disfavoring productive transcription of HIGs under normoxia.

These findings indicate that post-translational modifications of TOP2B by gene-specific transcription factors contribute to the modulation of TOP2B: TOP2B binding to and catalysis of its substrate DNA and TOP2B release from the resulting (product) DNA. Currently, the CTD of TOP2B, which is the hub of numerous modifications including acetylation, phosphorylation, methylation, sumoylation and ubiquitination etc. (https://www.phosphosite.org/proteinAction.action?id=5866&showAllSites=true), has not been structurally resolved, meaning that this domain is highly flexible, unstructured from the core domains[35]. It also suggests that TOP2B CTD composed of approximately 400 amino acids is available to interact with various transcription factors for the stepwise regulation of this enzyme. DNA is the paper for Pol II to copy and the road for Pol II to run and the DNA topology is key regulator for Pol II processivity and productivity. We propose that DNA-PK-mediated TOP2B phosphorylation and regulation in HIG transcription is an important, gene-specific topological element in Pol II transcription.

METHODS

Cell culture and conditions. Cell culture of SH-SY5Y and HCT116 cells were carried out as recommended by ATCC guidelines, maintaining the cells in DMEM-high glucose (Cytiva Hyclone, SH30243.01) and MEM alpha modification (Hyclone, SH30265.01), respectively, supplemented with 10% fetal bovine serum (FBS, Gibco) and 1% penicillin/streptomycin (P/S, Thermo Fisher). $CoCl_2$ (Cat. 60818, Sigma, USA), or H_2O as the control (–$CoCl_2$), was treated at a final concentration of 200 μM for 12–24 h. TOP2B inhibitors, ICRF193 (Sigma, I4659) and etoposide (Sigma, 341205) were used at a final concentration of 10 μM in 0.1% DMSO for 3 h.

Cloning and plasmid preparation. TOP2B plasmid encoding amino acids 1-1621 prepended by an HRV3C protease site[34] was used as a PCR template with primers that contain the desired mutations using the Quickchange kit (Stratagene) following the manufacturer's instruction. LR Clonase II (Thermo Fisher Scientific) was used to transfer the HRV3C-TOP2B mutant insert into pcDNA6.2/N-YFPDest to generate the YFP-TOP2B plasmid, transformed into the Stbl3 *E. coli* strain (Thermo Fisher Scientific), and purified using a Plasmid DNA Midiprep kit (Zymo Research). The insert was fully sequenced to confirm the absence of undesired mutations.

Cell transfection and knock-out cell preparation. TOP2B KO SH-SY5Y cells were previously generated[36] and gifted by Dr. C.A. Austin's group at Newcastle University in UK. DNA-PK KO or catalytic-null DNA-PK-expressing HCT116 cells were previously generated and characterized[62,63]. For the transfection of WT or mutant TOP2B variants, SH-SY5Y cells were grown to 60–70% confluence in a complete medium. The medium was replaced with Opti-MEM (Gibco, 31985) or with DMEM-high glucose without FBS and P/S before transfecting with the plasmids. Lipofectamine 2000 (Invitrogen) or FuGENE HD (Promega, E2311) transfection reagent was used according to the manufacturer's instructions. The transfected cells were collected after 50 h incubation for RNA or protein analyses and TMP-seq.

Quantitative reverse-transcription PCR (qRT-PCR). Total RNA was prepared using the RNeasy kit (Qiagen) following the manufacturer's instructions. The concentration of RNA samples was measured using Nanodrop and 0.6 μg of RNA was converted into cDNA using ReverTra Ace qPCR RT Master Mix (Toyobo). Quantitative PCR was conducted with equal amounts of resultant cDNAs, the indicated primers (**Table S1**), and SYBR Green PCR Master Mix (Applied Biosystems) using the StepOnePlus Real-Time PCR System (Applied Biosystems). β-Actin was used for normalization as a reference gene. Thermal cycles were as follows: 1 min at 95°C followed by 45 cycles of 15 s at 95°C, 15 s at 55°C, and 1 min at 72 °C. The results were presented as relative fold differences, standard deviations (SDs), and statistical validations (see below).

Chromatin immunoprecipitation and PCR/qPCR. ChIP-PCR or -qPCR analyses were conducted following the previously described methods and reagents without modifications[21,22,34]. The antibodies used for this study were TOP2B (A300-949A, Bethyl Laboratories), TOP2A (sc-365916, Santa Cruz Technologies), γH2AX (ab229914, Abcam), HIF1α (#14179, Cell Signaling Technology), DNA-PK (ab168854, Abcam), and pDNA-PK (T2609, ab124918, Abcam). The primer sets used are listed in **Table S1**.

Immunoblotting. HCT116 or SH-SY5Y cell extracts were prepared using a RIPA buffer (Cell Signaling Technology) in the presence of freshly added protease inhibitors [1 mM benzamidine, 0.25 mM PMSF, 1 mM Na-metabisulfite, 1 mM dithiothreitol (DTT); chemicals purchased from Sigma]. Protein concentrations in the cell extracts were determined by Bradford assays (Bio-Rad

Laboratories) using BSA standard curves. Detailed immunoprecipitation method description is available in our previous study[73]. The antibodies used for this study were DNA-PK (ab168854, Abcam), TOP2B (A300-950A, Bethyl Laboratories), γH2AX (ab229914, Abcam), ACTIN (β-ACTIN, MA5-15739, Invitrogen), and HIF1α (#14179, Cell Signaling Technology).

Immunoprecipitation. Protein A or G agarose beads (Prod # 20333, Pierce, Thermo Scientific; sc-2002, Santa Cruz Biotechnologies) were equilibrated with 0.15 M HEGN (50 mM HEPES, pH 7.6, 0.15 M KCl, 0.1 mM EDTA, 10% glycerol, 0.02% NP40). TOP2B (A300-950A, Bethyl Laboratories) or DNA-PK (ab168854, Abcam) antibodies were bound to the beads and incubated with the HeLa nuclear extracts (gift from Dr. D. J. Taatjes' laboratory at the University of Colorado)[34,35] for 90 min at 4°C. Control goat (NI02, EMD Millipore Corp.) and rabbit IgG (NB810-56910, Novus Biologicals) were used for DNA-PK and TOP2B immunoprecipitation, respectively. The bead-protein complexes were washed with a 33-bead volume of 0.5 M KCl-HEGN three times and then with the same volume of 0.15 M KCl-HEGN once at 4°C. All buffer solutions included fresh protease inhibitors described above and aprotinin (A6279, Sigma). The resultant pellet fractions were stored and subjected to immunoblotting analyses.

ICE assay. ICE assay was performed using the Human Topoisomerase ICE Assay Kit (TG1020-2b, Topogen), according to the manufacturer's instruction. Cells were grown to about 70% confluence in 6-well plates and treated with 200 μM $CoCl_2$ or the same amount of H_2O for 12 h. DMSO (control, –Eto) or 50 μM etoposide was supplemented for 1 h, prior to harvesting the cells for the ICE assay, followed by immunoblotting using TOP2B (A300-950A, Bethyl Laboratories) and TOP2A (sc-365916, Santa Cruz Technologies) antibodies.

RNA-sequencing (RNA-seq). WT and DNA-PK KO HCT116 cells were grown to approximately 60% confluence before supplementing $CoCl_2$ to a final concentration of 200 μM for 12 h. Cells were collected and total RNAs were extracted from the cells and purified using RNeasy kit (Qiagen). cDNA construction and sequencing were performed by Omega Bioservices as previously described[74].

Trimethylpsoralen-sequencing (TMP-seq). Preparation of TMP DNA samples for sequencing was adapted and modified from a previous study[75]. WT, TOP2B KO, and TOP2B mutant-expressing

TOP2B KO cells were grown to approximately 80% confluence. When indicated, $CoCl_2$ was treated to a final concentration of 200 μM for 24 h. TMP (T6137, Sigma), an intercalating chemical that can covalently cross-link negatively supercoiled DNA, was supplemented to each cell plate at a final concentration of 2 μg/mL for 10 min before cross-linking DNA by 360 nm light at a dose of 1.2 kJ/m^2/min for 2 min. Cells were washed with cold PBS twice and collected by scraping. Cells were resuspended in PBS including 0.5% SDS. Proteinase K, 4 μg/each sample, was supplemented and the mixture was incubated at 55°C for 1 h, followed by sonication to obtain the genomic DNA, optimally, into 300–700 bp fragments. The samples were subjected to phenol-chloroform-isoamyl ethanol (PCI) extraction and ethanol precipitation. RNAs were digested by RNase A, 1 μg/each sample, remaining only DNA, and the DNA was recovered by PCI extraction and ethanol precipitation. The DNA concentration was measured and 40 μg of DNA per sample was taken to the next steps. The volumes of samples were adjusted to be equal. The samples were boiled for 10 min and then put on ice for 2 min, followed by *E. coli* exonuclease I digestion at 37°C for 1 h. The boiling, chilling, and exonuclease I digestion were repeated once more. Remaining, cross-linked DNA was purified by PCR purification kit (Qiagen) and reverse-crosslinked by BCR reversal with 0.1 M KOH, heating at 90°C for 30 min and neutralization with 3 M sodium acetate, pH 7.0. The resultant DNA was purified using PCR purification kit (Qiagen), visualized on agarose gels, and analyzed by next generation sequencing (NGS) and bioinformatics. The xGen ssDNA sequencing libraries were prepared according to the manufacturer's instructions of xGen ssDNA & Low-Input DNA Library Prep Kit (Integrated DNA Technologies). In summary, 100 ng of ssDNA was sheared using adaptive focused acoustic technology (Covaris) to a target peak size of 350 bp. The denatured ssDNA fragments underwent tailing and ligation with R2 stubby adapter to the 3' end. After the initial ligation, the ssDNA was converted into a double-stranded form through an extension process. Additionally, the R1 stubby adapter was ligated at the 5' end of these DNA fragments. Subsequently, the indexes were attached using PCR for Illumina sequencing. The libraries were quantified using qPCR according to the qPCR Quantification Protocol Guide (KAPA Library Quantification kits for Illumina Sequencing platforms) and assessed for quality using Agilent Technologies 4200 TapeStation HSD1000 ScreenTape (Agilent technologies). Paired-end sequencing was then conducted using the NovaSeq X platform (Illumina).

Bioinformatics. For RNA-seq, sequenced reads (paired-end) in FASTQ format were trimmed using Trim Galore (version 0.6.6) with Cutadapt (version 3.4) and their quality was assured using FastQC (version 0.11.9). Quality-assured trimmed reads were then aligned to the reference genome (hg38 assembly) using STAR (version 2.7.9a) with the following parameters: --outSAMtype BAM SortedByCoordinate, --quantMode TranscriptomeSAM, and --outFilterMultimapNmax 1. The integrity of transcripts was evaluated by means of transcript integrity number (TIN) scores using RseQC (tin.py, version 4.0.0). Gene expression levels were quantified using StringTie (version 2.1.7b), and differential gene expression analysis was conducted using DESeq2 (version 1.36.0) to identify genes with significant changes between conditions. For TMP-seq, the procedures up to the alignment step were the same as described above. Normalized coverage profiles were generated from the aligned reads (BAM files) using bamCoverage in deepTools (version 3.5.3). The reads per kilobase per million mapped reads (RPKM) method was used for normalization. To merge replicates, bigwigCompare in deepTools was used with the mean operation to calculate the average signal across replicates. Heatmaps representing TMP-seq signal intensities were generated using plotHeatmap in deepTools. Line plots comparing TMP-seq signals between conditions were generated using plotProfile in deepTools.

Statistics and Reproducibility. Standard deviation was calculated and used to generate error bars. The Student's t-test ($p < 0.05$, one-sided) or one-way ANOVA with multiple comparison was used to determine statistical significance. Graphs were generated using the Prism 9 software (GraphPad, Inc.). Representative experimental images of gels and autographs were repeated at least twice independently with similar results.

Data Availability

All data are available in the manuscript or as supplementary information. Source data are provided with this paper. The RNA-seq and TMP-seq data generated in this study have been deposited in the under accession codes GSE285698 and GSE285699, respectively.

Acknowledgments

We are grateful to C. A. Austin at Newcastle University in the United Kingdom for sharing the TOP2B KO SH-SY5Y cells and to D. J. Taatjes at the University of Colorado at Boulder for sharing the HeLa

nuclear extracts. We also thank Rokit Genomics in S. Korea and S. Ju, J. Jeong, and the current members of the Bunch laboratory members at KNU for their technical assistance. H.B. thanks J. N. Park, S. W. Yang, John and D. Y. Bunch and J. Christ for their loving encouragement and support throughout the course of this work. This research was supported by grants from Thomas H. and Dorthy S. Corson Career Development Award in Cardiovascular Disease Research, funded by the Center for Clinical and Translational Science, Mayo Clinic to M.J.S., from the Korea Health Technology R&D Project through Korea Health Industry Development Institute (KHIDI), funded by the Ministry of Health, & Welfare of the Republic of Korea (R5-2024-00437643) to J.J., and from the National Research Foundation (NRF) of the Republic of Korea (2022R1A21003569) to H.B.

Author Contributions

HB, MS, and JL performed ChIP-PCR/qPCR and qRT-PCR. JP and KK carried out bioinformatics analyses. JF and M(J)S designed, cloned, and prepared WT and mutant TOP2B plasmids for transfection. HL and AD prepared and cultured DNA-PK KO and mutant HCT116 cells. HB performed ICE assay, immunoprecipitation, and immunoblotting. HB and J-SY carried out mammalian transfection. HB prepared for the samples for RNA-seq and TMP-seq. JJ, YY, SC, KK, and HB performed the genomic data analysis and revised the manuscript. HB created the hypothesis, designed and coordinated the experiments, analyzed and curated the data, and wrote and revised the manuscript.

Competing Interests Statement

The authors declare that they have no competing interests.

References

1 Schier, A. C. & Taatjes, D. J. Structure and mechanism of the RNA polymerase II transcription machinery. *Genes Dev* **34**, 465-488, doi:10.1101/gad.335679.119 (2020).

2 Roeder, R. G. 50+ years of eukaryotic transcription: an expanding universe of factors and mechanisms. *Nat Struct Mol Biol* **26**, 783-791, doi:10.1038/s41594-019-0287-x (2019).

3 Bunch, H. in *Heat Shock Proteins in Inflammatory Diseases* (eds Alexzander A. A. Asea & Punit Kaur) 489-508 (Springer International Publishing, 2021).

4 Muniz, L., Nicolas, E. & Trouche, D. RNA polymerase II speed: a key player in controlling and adapting transcriptome composition. *EMBO J* **40**, e105740, doi:10.15252/embj.2020105740 (2021).

5 Lee, P., Chandel, N. S. & Simon, M. C. Cellular adaptation to hypoxia through hypoxia inducible factors and beyond. *Nat Rev Mol Cell Biol* **21**, 268-283, doi:10.1038/s41580-020-0227-y (2020).
6 Nelson, D. L. *Lehninger principles of biochemistry*. (Fourth edition. New York : W.H. Freeman, 2005., 2005).
7 Greijer, A. E. & van der Wall, E. The role of hypoxia inducible factor 1 (HIF-1) in hypoxia induced apoptosis. *J Clin Pathol* **57**, 1009-1014, doi:10.1136/jcp.2003.015032 (2004).
8 Koyasu, S., Kobayashi, M., Goto, Y., Hiraoka, M. & Harada, H. Regulatory mechanisms of hypoxia-inducible factor 1 activity: Two decades of knowledge. *Cancer Sci* **109**, 560-571, doi:10.1111/cas.13483 (2018).
9 Ma, Z. *et al.* Targeting hypoxia-inducible factor-1, for cancer treatment: Recent advances in developing small-molecule inhibitors from natural compounds. *Semin Cancer Biol* **80**, 379-390, doi:10.1016/j.semcancer.2020.09.011 (2022).
10 Wu, Q. *et al.* Hypoxia-inducible factors: master regulators of hypoxic tumor immune escape. *J Hematol Oncol* **15**, 77, doi:10.1186/s13045-022-01292-6 (2022).
11 Kierans, S. J. & Taylor, C. T. Regulation of glycolysis by the hypoxia-inducible factor (HIF): implications for cellular physiology. *J Physiol* **599**, 23-37, doi:10.1113/JP280572 (2021).
12 Rana, N. K., Singh, P. & Koch, B. CoCl(2) simulated hypoxia induce cell proliferation and alter the expression pattern of hypoxia associated genes involved in angiogenesis and apoptosis. *Biol Res* **52**, 12, doi:10.1186/s40659-019-0221-z (2019).
13 Hsu, C. W. *et al.* Identification of approved and investigational drugs that inhibit hypoxia-inducible factor-1 signaling. *Oncotarget* **7**, 8172-8183, doi:10.18632/oncotarget.6995 (2016).
14 Hubbi, M. E. & Semenza, G. L. Regulation of cell proliferation by hypoxia-inducible factors. *Am J Physiol Cell Physiol* **309**, C775-782, doi:10.1152/ajpcell.00279.2015 (2015).
15 Marxsen, J. H. *et al.* Hypoxia-inducible factor-1 (HIF-1) promotes its degradation by induction of HIF-alpha-prolyl-4-hydroxylases. *Biochem J* **381**, 761-767, doi:10.1042/BJ20040620 (2004).
16 Nakayama, K. *et al.* Large-scale mapping of positional changes of hypoxia-responsive genes upon activation. *Mol Biol Cell* **33**, ar72, doi:10.1091/mbc.E21-11-0593 (2022).
17 Chaplin, A. K. *et al.* Dimers of DNA-PK create a stage for DNA double-strand break repair. *Nat Struct Mol Biol* **28**, 13-19, doi:10.1038/s41594-020-00517-x (2021).
18 Fowler, F. C. *et al.* DNA-PK promotes DNA end resection at DNA double strand breaks in G(0) cells. *Elife* **11**, doi:10.7554/eLife.74700 (2022).
19 Convery, E. *et al.* Inhibition of homologous recombination by variants of the catalytic subunit of the DNA-dependent protein kinase (DNA-PKcs). *Proc Natl Acad Sci U S A* **102**, 1345-1350, doi:10.1073/pnas.0406466102 (2005).
20 Deshpande, R. A. *et al.* DNA-dependent protein kinase promotes DNA end processing by MRN and CtIP. *Sci Adv* **6**, eaay0922, doi:10.1126/sciadv.aay0922 (2020).
21 Bunch, H. *et al.* TRIM28 regulates RNA polymerase II promoter-proximal pausing and pause release. *Nat Struct Mol Biol* **21**, 876-883, doi:10.1038/nsmb.2878 (2014).
22 Bunch, H. *et al.* Transcriptional elongation requires DNA break-induced signalling. *Nat Commun* **6**, 10191, doi:10.1038/ncomms10191 (2015).
23 Bunch, H. & Calderwood, S. K. TRIM28 as a novel transcriptional elongation factor. *BMC Mol Biol* **16**, 14, doi:10.1186/s12867-015-0040-x (2015).
24 Bunch, H. Role of genome guardian proteins in transcriptional elongation. *FEBS Lett* **590**, 1064-1075, doi:10.1002/1873-3468.12152 (2016).

25 Galbraith, M. D. *et al.* HIF1A employs CDK8-mediator to stimulate RNAPII elongation in response to hypoxia. *Cell* **153**, 1327-1339, doi:10.1016/j.cell.2013.04.048 (2013).
26 Yang, Y. *et al.* HIF-1 Interacts with TRIM28 and DNA-PK to release paused RNA polymerase II and activate target gene transcription in response to hypoxia. *Nat Commun* **13**, 316, doi:10.1038/s41467-021-27944-8 (2022).
27 Nitiss, J. L. DNA topoisomerase II and its growing repertoire of biological functions. *Nat Rev Cancer* **9**, 327-337, doi:10.1038/nrc2608 (2009).
28 Cuvier, O. & Hirano, T. A role of topoisomerase II in linking DNA replication to chromosome condensation. *J Cell Biol* **160**, 645-655, doi:10.1083/jcb.200209023 (2003).
29 Haffner, M. C. *et al.* Androgen-induced TOP2B-mediated double-strand breaks and prostate cancer gene rearrangements. *Nature genetics* **42**, 668-675, doi:10.1038/ng.613 (2010).
30 Williamson, L. M. & Lees-Miller, S. P. Estrogen receptor alpha-mediated transcription induces cell cycle-dependent DNA double-strand breaks. *Carcinogenesis* **32**, 279-285, doi:10.1093/carcin/bgq255 (2011).
31 Sasanuma, H. *et al.* BRCA1 ensures genome integrity by eliminating estrogen-induced pathological topoisomerase II-DNA complexes. *Proc Natl Acad Sci U S A* **115**, E10642-E10651, doi:10.1073/pnas.1803177115 (2018).
32 Ju, B. G. *et al.* A topoisomerase IIbeta-mediated dsDNA break required for regulated transcription. *Science* **312**, 1798-1802, doi:10.1126/science.1127196 (2006).
33 Madabhushi, R. *et al.* Activity-Induced DNA Breaks Govern the Expression of Neuronal Early-Response Genes. *Cell* **161**, 1592-1605, doi:10.1016/j.cell.2015.05.032 (2015).
34 Bunch, H. *et al.* BRCA1-BARD1 regulates transcription through modulating topoisomerase IIbeta. *Open Biol* **11**, 210221, doi:10.1098/rsob.210221 (2021).
35 Bunch, H. *et al.* ERK2-topoisomerase II regulatory axis is important for gene activation in immediate early genes. *Nat Commun* **14**, 8341, doi:10.1038/s41467-023-44089-y (2023).
36 Khazeem, M. M. *et al.* TOP2B Is Required to Maintain the Adrenergic Neural Phenotype and for ATRA-Induced Differentiation of SH-SY5Y Neuroblastoma Cells. *Mol Neurobiol* **59**, 5987-6008, doi:10.1007/s12035-022-02949-6 (2022).
37 Mizutani, M., Ohta, T., Watanabe, H., Handa, H. & Hirose, S. Negative supercoiling of DNA facilitates an interaction between transcription factor IID and the fibroin gene promoter. *Proc Natl Acad Sci U S A* **88**, 718-722, doi:10.1073/pnas.88.3.718 (1991).
38 Ma, J. & Wang, M. D. DNA supercoiling during transcription. *Biophys Rev* **8**, 75-87, doi:10.1007/s12551-016-0215-9 (2016).
39 Wu, H. Y., Shyy, S. H., Wang, J. C. & Liu, L. F. Transcription generates positively and negatively supercoiled domains in the template. *Cell* **53**, 433-440, doi:10.1016/0092-8674(88)90163-8 (1988).
40 Guo, M. S., Kawamura, R., Littlehale, M. L., Marko, J. F. & Laub, M. T. High-resolution, genome-wide mapping of positive supercoiling in chromosomes. *Elife* **10**, doi:10.7554/eLife.67236 (2021).
41 Ma, J., Bai, L. & Wang, M. D. Transcription under torsion. *Science* **340**, 1580-1583, doi:10.1126/science.1235441 (2013).
42 Patel, H. P. *et al.* DNA supercoiling restricts the transcriptional bursting of neighboring eukaryotic genes. *Mol Cell* **83**, 1573-1587 e1578, doi:10.1016/j.molcel.2023.04.015 (2023).
43 Abbasi, S. & Schild-Poulter, C. Mapping the Ku Interactome Using Proximity-Dependent Biotin Identification in Human Cells. *J Proteome Res* **18**, 1064-1077, doi:10.1021/acs.jproteome.8b00771 (2019).

44 Muslimovic, A., Nystrom, S., Gao, Y. & Hammarsten, O. Numerical analysis of etoposide induced DNA breaks. *PLoS One* **4**, e5859, doi:10.1371/journal.pone.0005859 (2009).
45 Yao, Q., Zhu, L., Shi, Z., Banerjee, S. & Chen, C. Topoisomerase-modulated genome-wide DNA supercoiling domains colocalize with nuclear compartments and regulate human gene expression. *Nat Struct Mol Biol*, doi:10.1038/s41594-024-01377-5 (2024).
46 Pedersen, J. M. *et al.* DNA Topoisomerases maintain promoters in a state competent for transcriptional activation in Saccharomyces cerevisiae. *PLoS Genet* **8**, e1003128, doi:10.1371/journal.pgen.1003128 (2012).
47 Puc, J., Aggarwal, A. K. & Rosenfeld, M. G. Physiological functions of programmed DNA breaks in signal-induced transcription. *Nat Rev Mol Cell Biol* **18**, 471-476, doi:10.1038/nrm.2017.43 (2017).
48 Teves, S. S. & Henikoff, S. DNA torsion as a feedback mediator of transcription and chromatin dynamics. *Nucleus* **5**, 211-218, doi:10.4161/nucl.29086 (2014).
49 Szlachta, K. *et al.* Alternative DNA secondary structure formation affects RNA polymerase II promoter-proximal pausing in human. *Genome Biol* **19**, 89, doi:10.1186/s13059-018-1463-8 (2018).
50 Skourti-Stathaki, K. & Proudfoot, N. J. A double-edged sword: R loops as threats to genome integrity and powerful regulators of gene expression. *Genes Dev* **28**, 1384-1396, doi:10.1101/gad.242990.114 (2014).
51 Jha, R. K., Levens, D. & Kouzine, F. Mechanical determinants of chromatin topology and gene expression. *Nucleus* **13**, 94-115, doi:10.1080/19491034.2022.2038868 (2022).
52 Pommier, Y., Sun, Y., Huang, S. N. & Nitiss, J. L. Roles of eukaryotic topoisomerases in transcription, replication and genomic stability. *Nat Rev Mol Cell Biol* **17**, 703-721, doi:10.1038/nrm.2016.111 (2016).
53 Chen, C., Pore, N., Behrooz, A., Ismail-Beigi, F. & Maity, A. Regulation of glut1 mRNA by hypoxia-inducible factor-1. Interaction between H-ras and hypoxia. *J Biol Chem* **276**, 9519-9525, doi:10.1074/jbc.M010144200 (2001).
54 Hayashi, M. *et al.* Induction of glucose transporter 1 expression through hypoxia-inducible factor 1alpha under hypoxic conditions in trophoblast-derived cells. *J Endocrinol* **183**, 145-154, doi:10.1677/joe.1.05599 (2004).
55 Jin, X. *et al.* A positive feedback circuit comprising p21 and HIF-1alpha aggravates hypoxia-induced radioresistance of glioblastoma by promoting Glut1/LDHA-mediated glycolysis. *FASEB J* **36**, e22229, doi:10.1096/fj.202101736R (2022).
56 Triantafyllou, A. *et al.* Cobalt induces hypoxia-inducible factor-1alpha (HIF-1alpha) in HeLa cells by an iron-independent, but ROS-, PI-3K- and MAPK-dependent mechanism. *Free Radic Res* **40**, 847-856, doi:10.1080/10715760600730810 (2006).
57 Tripathi, V. K., Subramaniyan, S. A. & Hwang, I. Molecular and Cellular Response of Co-cultured Cells toward Cobalt Chloride (CoCl(2))-Induced Hypoxia. *ACS Omega* **4**, 20882-20893, doi:10.1021/acsomega.9b01474 (2019).
58 Herrero-Ruiz, A. *et al.* Topoisomerase IIalpha represses transcription by enforcing promoter-proximal pausing. *Cell Rep* **35**, 108977, doi:10.1016/j.celrep.2021.108977 (2021).
59 Das, S. K. *et al.* MYC assembles and stimulates topoisomerases 1 and 2 in a "topoisome". *Mol Cell* **82**, 140-158 e112, doi:10.1016/j.molcel.2021.11.016 (2022).
60 Calderwood, S. K. A critical role for topoisomerase IIb and DNA double strand breaks in transcription. *Transcription* **7**, 75-83, doi:10.1080/21541264.2016.1181142 (2016).
61 Aparicio, T., Baer, R., Gottesman, M. & Gautier, J. MRN, CtIP, and BRCA1 mediate repair of topoisomerase II-DNA adducts. *J Cell Biol* **212**, 399-408, doi:10.1083/jcb.201504005 (2016).

62 Lu, H., Saha, J., Beckmann, P. J., Hendrickson, E. A. & Davis, A. J. DNA-PKcs promotes chromatin decondensation to facilitate initiation of the DNA damage response. *Nucleic Acids Res* **47**, 9467-9479, doi:10.1093/nar/gkz694 (2019).
63 Lu, H. *et al.* DNA-PKcs-dependent phosphorylation of RECQL4 promotes NHEJ by stabilizing the NHEJ machinery at DNA double-strand breaks. *Nucleic Acids Res* **50**, 5635-5651, doi:10.1093/nar/gkac375 (2022).
64 Quintero-Fabian, S. *et al.* Role of Matrix Metalloproteinases in Angiogenesis and Cancer. *Front Oncol* **9**, 1370, doi:10.3389/fonc.2019.01370 (2019).
65 Cheung, E. C., Ludwig, R. L. & Vousden, K. H. Mitochondrial localization of TIGAR under hypoxia stimulates HK2 and lowers ROS and cell death. *Proc Natl Acad Sci U S A* **109**, 20491-20496, doi:10.1073/pnas.1206530109 (2012).
66 Foldager, C. B. *et al.* Validation of suitable house keeping genes for hypoxia-cultured human chondrocytes. *BMC Mol Biol* **10**, 94, doi:10.1186/1471-2199-10-94 (2009).
67 Foltyn, M. *et al.* The physiological mTOR complex 1 inhibitor DDIT4 mediates therapy resistance in glioblastoma. *Br J Cancer* **120**, 481-487, doi:10.1038/s41416-018-0368-3 (2019).
68 Jaskiewicz, M. *et al.* The transition from HIF-1 to HIF-2 during prolonged hypoxia results from reactivation of PHDs and HIF1A mRNA instability. *Cell Mol Biol Lett* **27**, 109, doi:10.1186/s11658-022-00408-7 (2022).
69 Zhao, J., Du, F., Shen, G., Zheng, F. & Xu, B. The role of hypoxia-inducible factor-2 in digestive system cancers. *Cell Death Dis* **6**, e1600, doi:10.1038/cddis.2014.565 (2015).
70 Naughton, C. *et al.* Transcription forms and remodels supercoiling domains unfolding large-scale chromatin structures. *Nat Struct Mol Biol* **20**, 387-395, doi:10.1038/nsmb.2509 (2013).
71 Liu, L. *et al.* Autophosphorylation transforms DNA-PK from protecting to processing DNA ends. *Mol Cell* **82**, 177-189 e174, doi:10.1016/j.molcel.2021.11.025 (2022).
72 Morotomi-Yano, K., Saito, S., Adachi, N. & Yano, K. I. Dynamic behavior of DNA topoisomerase IIbeta in response to DNA double-strand breaks. *Sci Rep* **8**, 10344, doi:10.1038/s41598-018-28690-6 (2018).
73 Jeong, J. *et al.* Lactiplantibacillus plantarum K8 lysates regulate hypoxia-induced gene expression. *Sci Rep* **14**, 6275, doi:10.1038/s41598-024-56958-7 (2024).
74 Kim, D. *et al.* Arsenic hexoxide has differential effects on cell proliferation and genome-wide gene expression in human primary mammary epithelial and MCF7 cells. *Sci Rep* **11**, 3761, doi:10.1038/s41598-021-82551-3 (2021).
75 Teves, S. S. & Henikoff, S. Transcription-generated torsional stress destabilizes nucleosomes. *Nat Struct Mol Biol* **21**, 88-94, doi:10.1038/nsmb.2723 (2014).

Figures

Fig. 1.

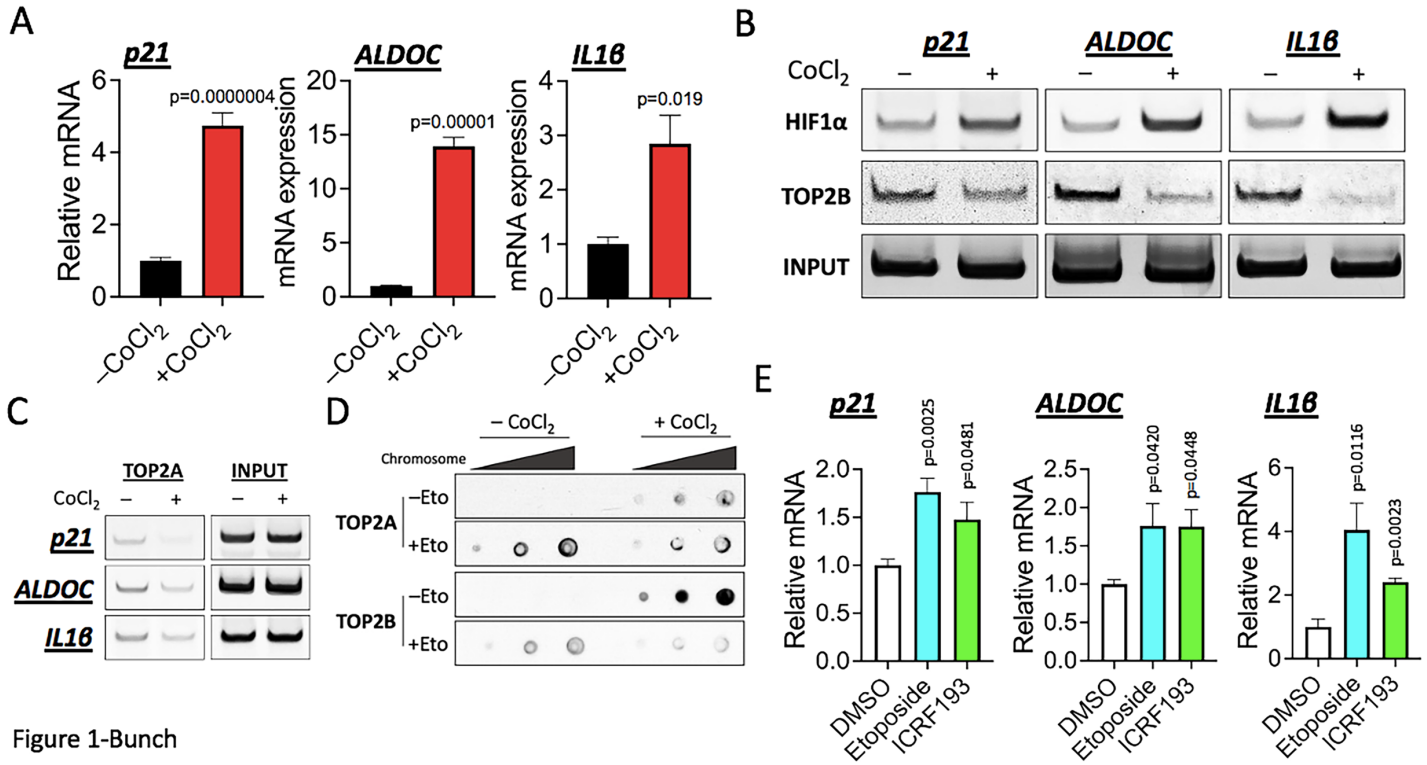

Figure 1-Bunch

Fig. 2.

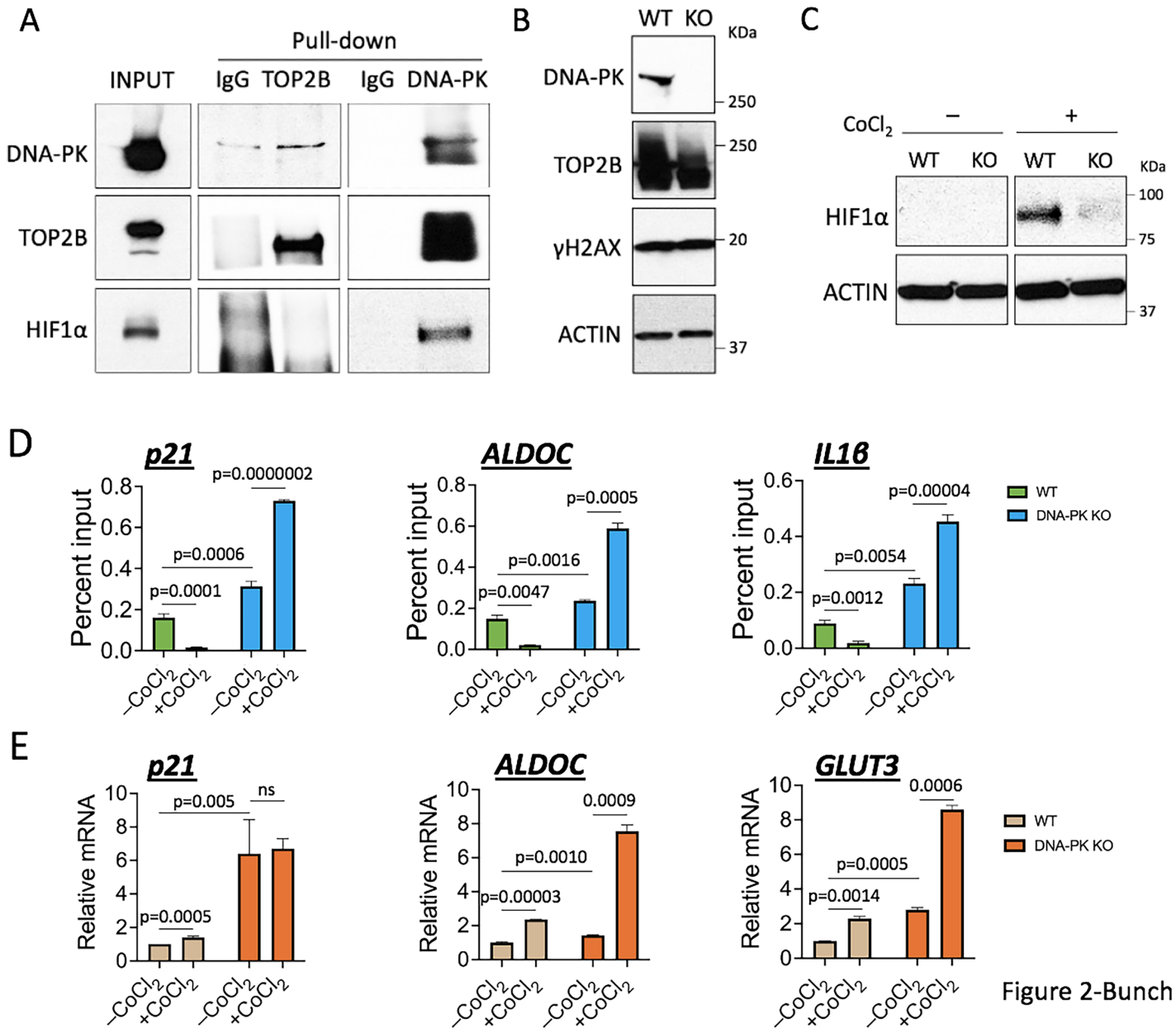

Figure 2-Bunch

Fig. 3.

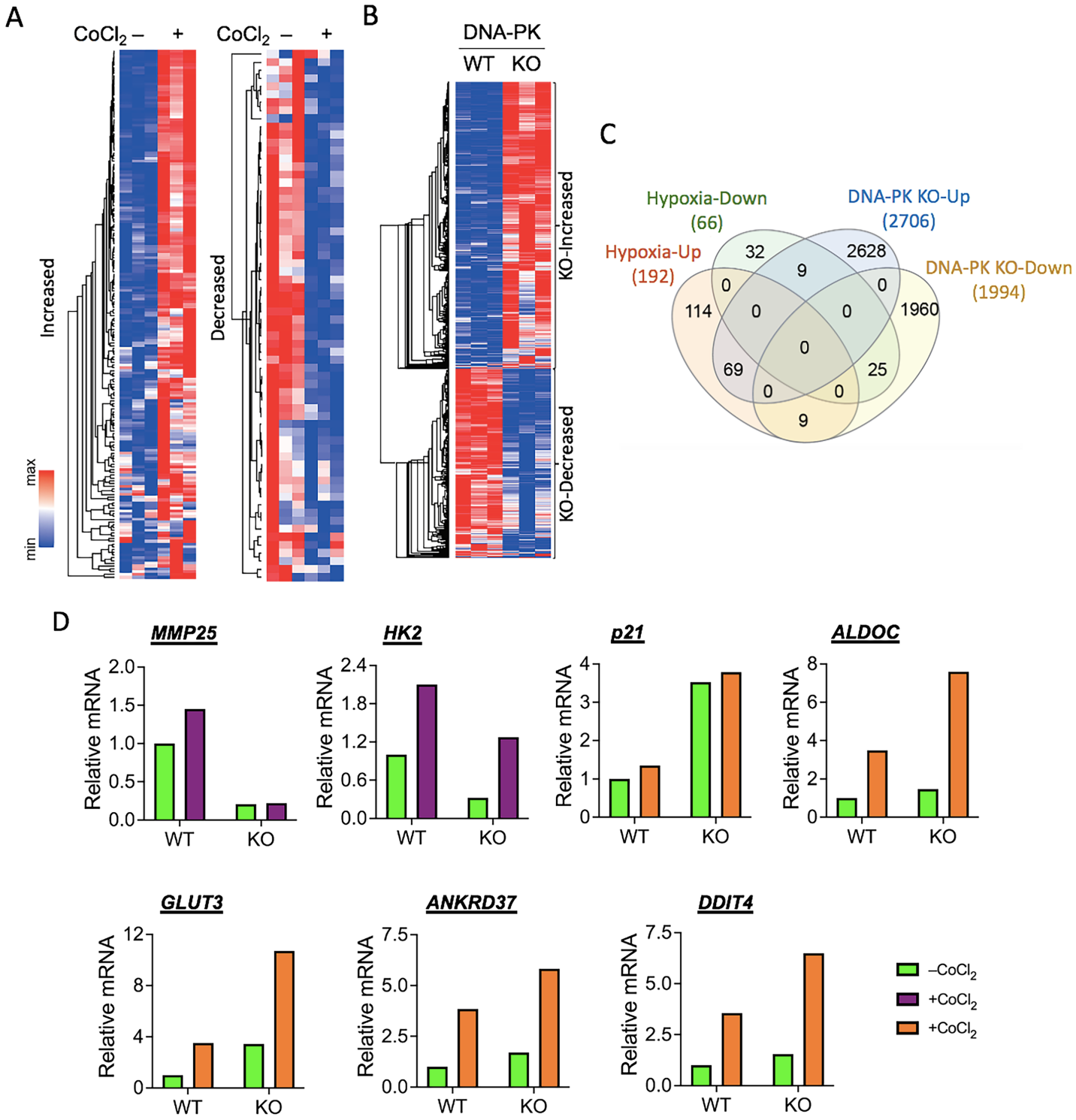
A
CoCl2 – +
CoCl2 – +
Increased
Decreased
max
min
B
DNA-PK
WT KO
KO-Increased
KO-Decreased
C
Hypoxia-Down
(66)
DNA-PK KO-Up
(2706)
Hypoxia-Up
(192)
DNA-PK KO-Down
(1994)
32
2628
9
0
0
114
0
0
1960
0
69
25
0
0
9
D
MMP25
HK2
p21
ALDOC
GLUT3
ANKRD37
DDIT4
Relative mRNA
WT
KO
–CoCl2
+CoCl2
+CoCl2

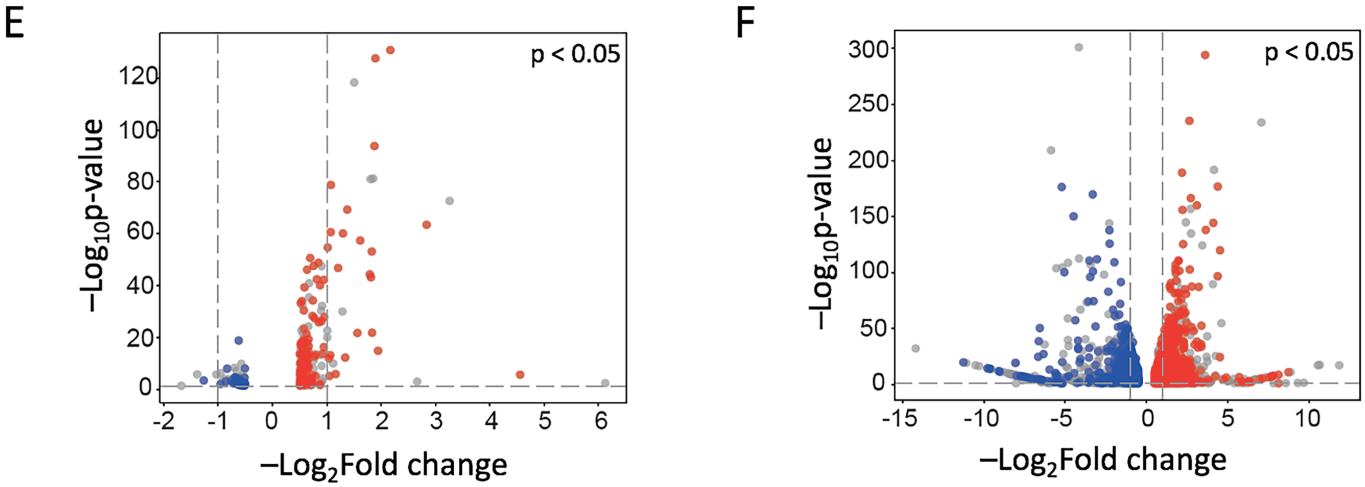

Figure 3-Bunch

Fig. 4.

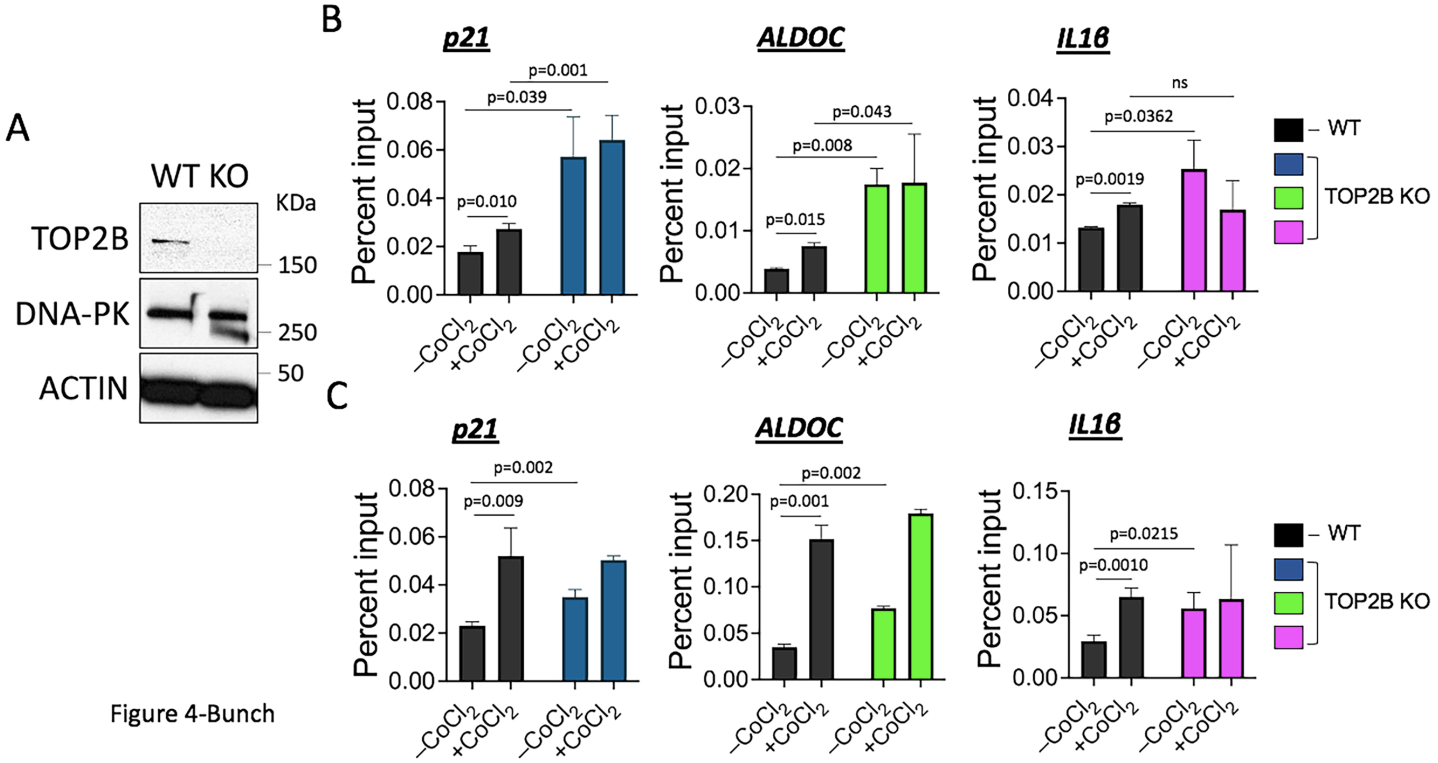

Figure 4-Bunch

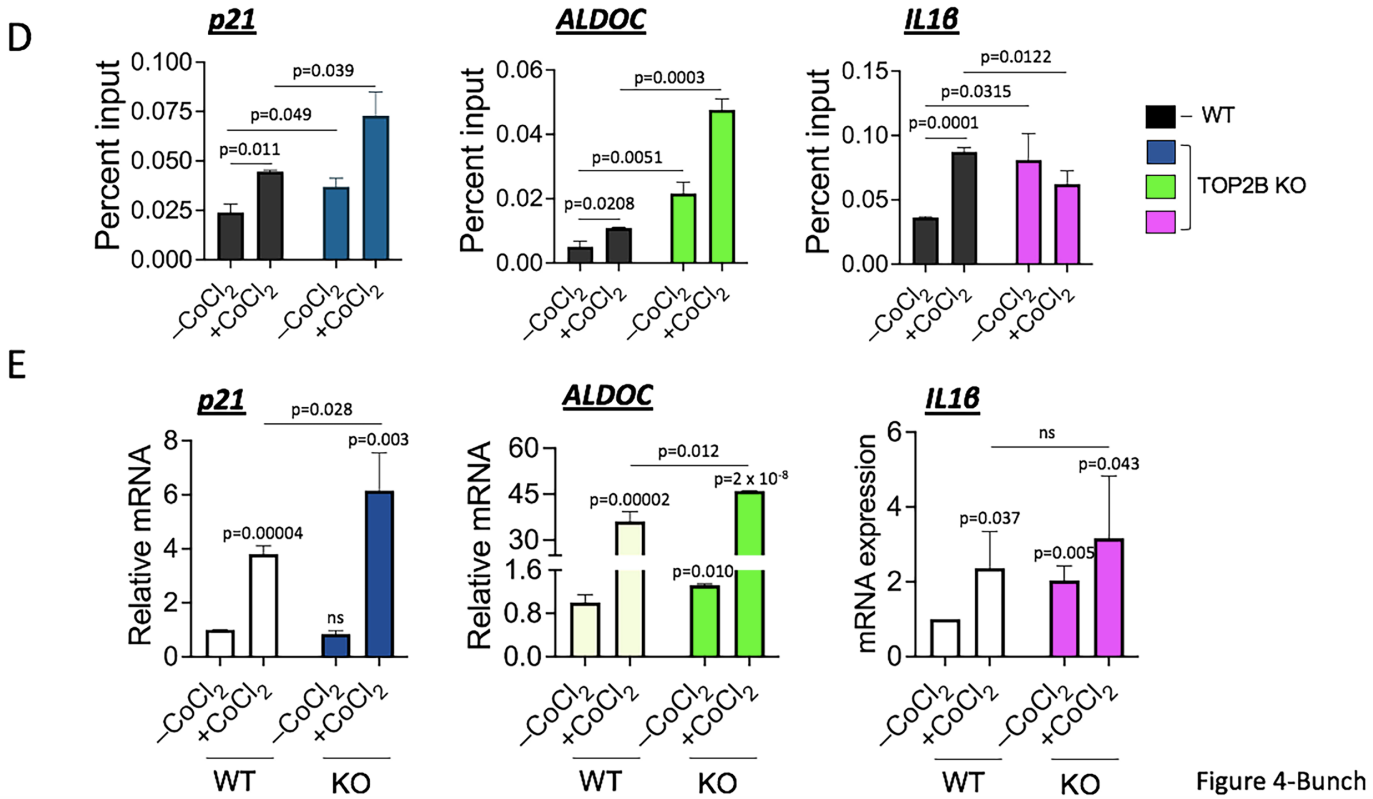

Figure 4-Bunch

Fig. 5.

A

Peptide	Primary Sequence	Mutation
1	^{1370}YTFDFSEEEDDDADDDDDDNNDLEELK^{1396}	
2	^{1399}ASPITNDGEDEFVPSDGLDK^{1418}	S1400A, T1403A
3	^{1464}FDSNEEDSASVFSPSFG LK^{1482}	
4	^{1516}VVEAVNSDSDSEFGIPK^{1532}	S1524A, S1526A
5	^{1548}KASGSENEGDYNPGR^{1562}	
6	^{1574}KTSFDQDSDVDIFPSDFPTEPPSLPR^{1599}	S1581A

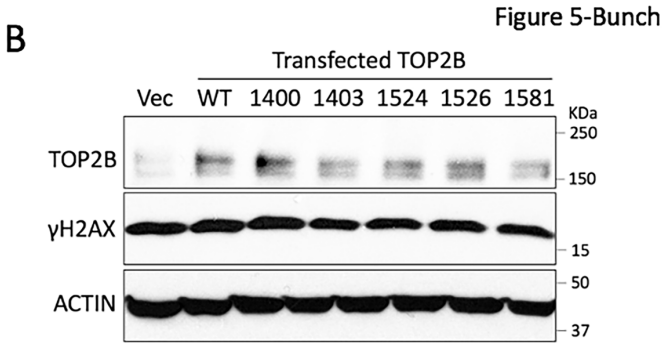

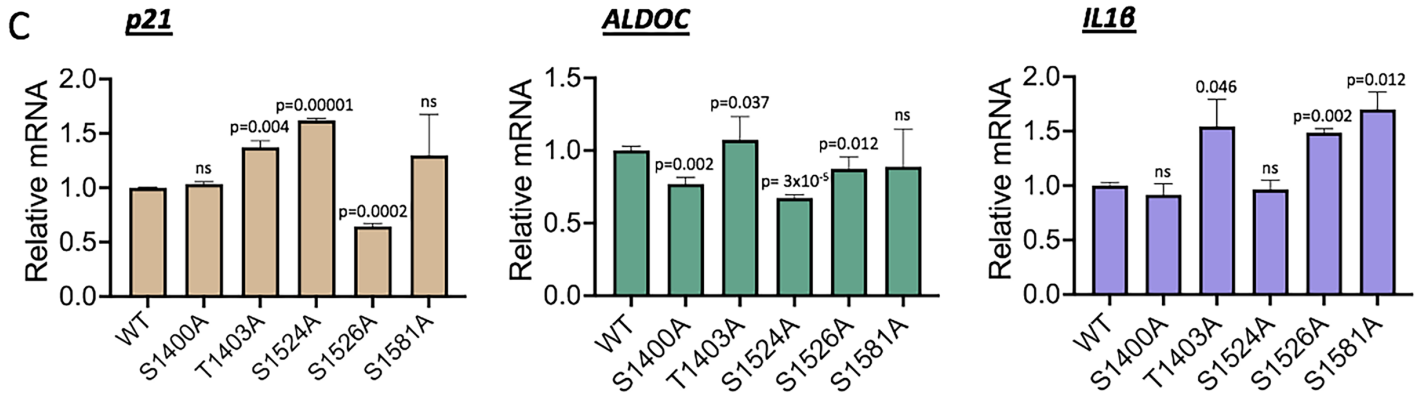

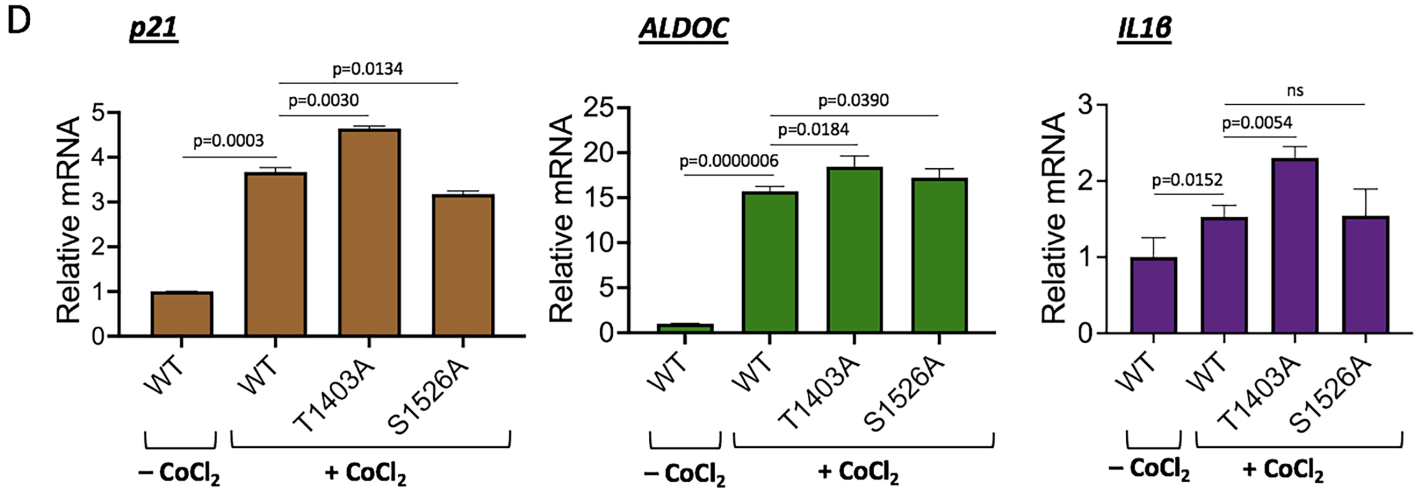

Fig. 6.

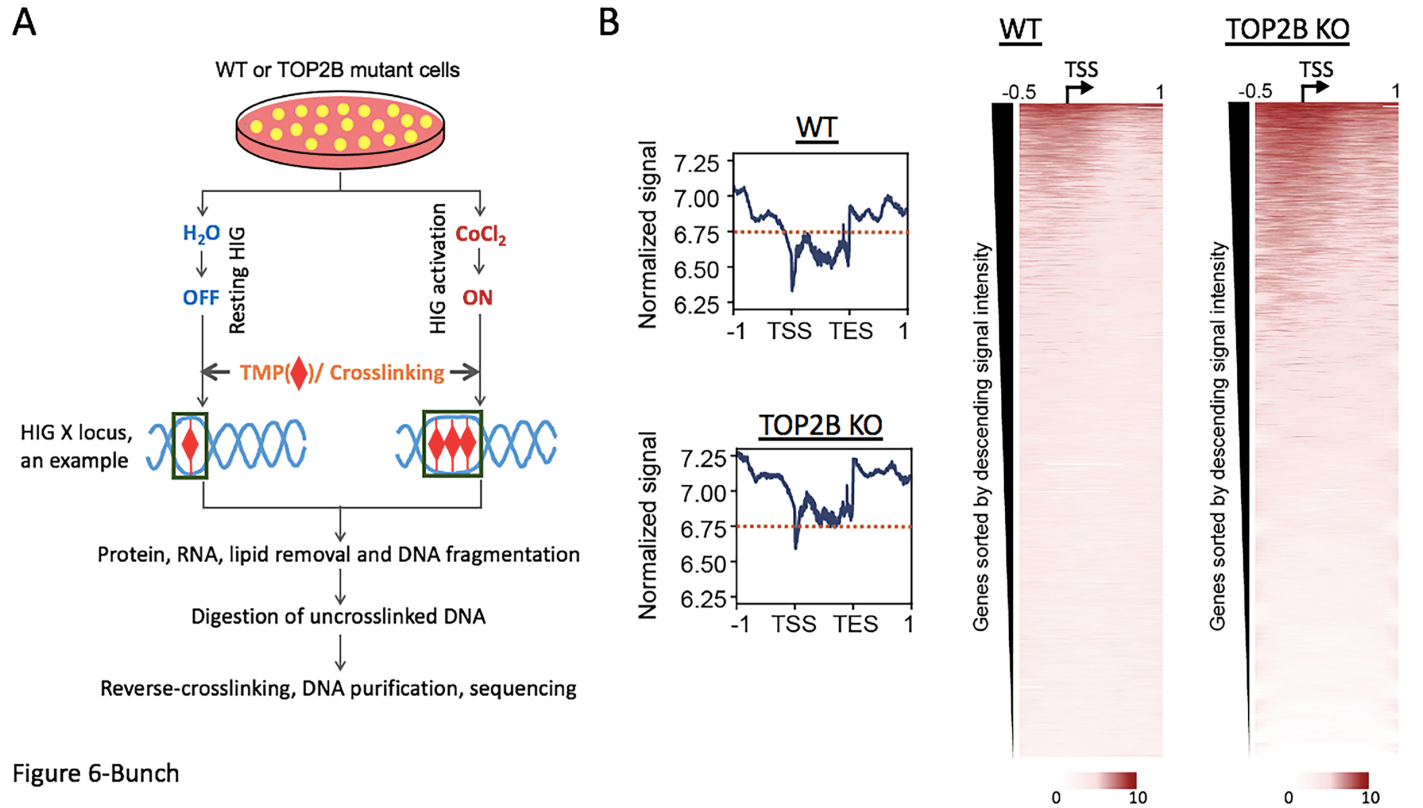

Figure 6-Bunch

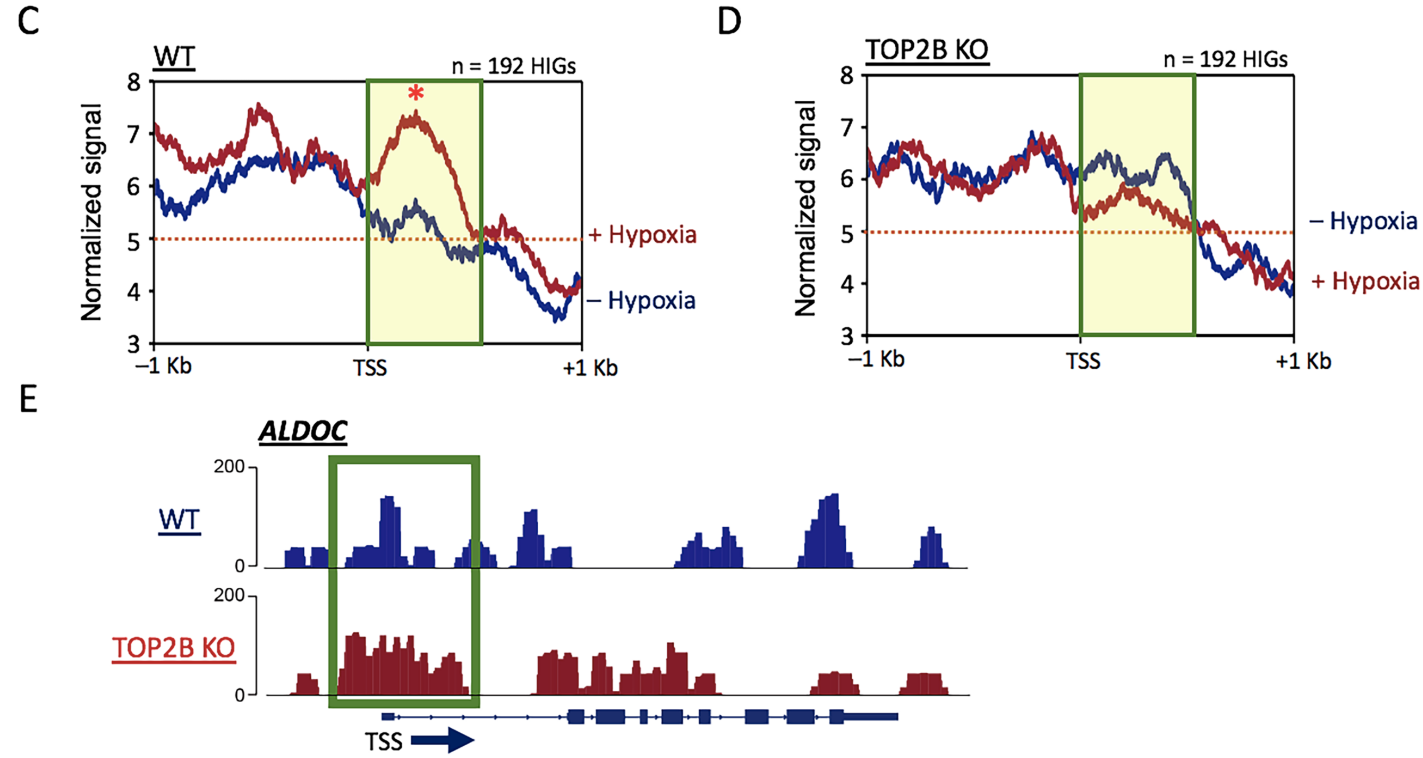

Figure 6-Bunch

F

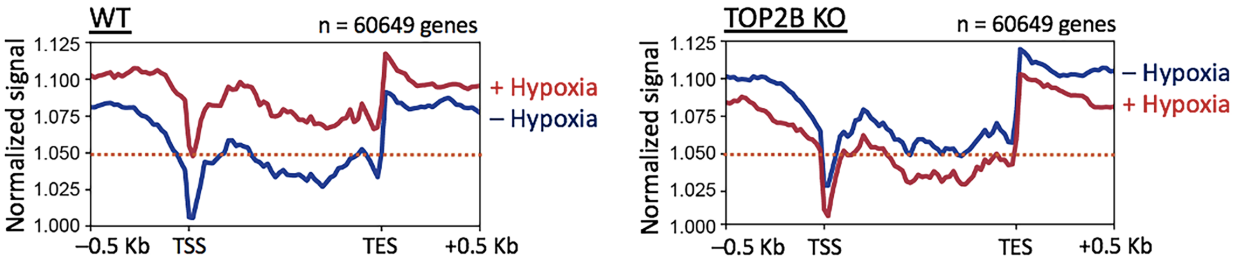

G

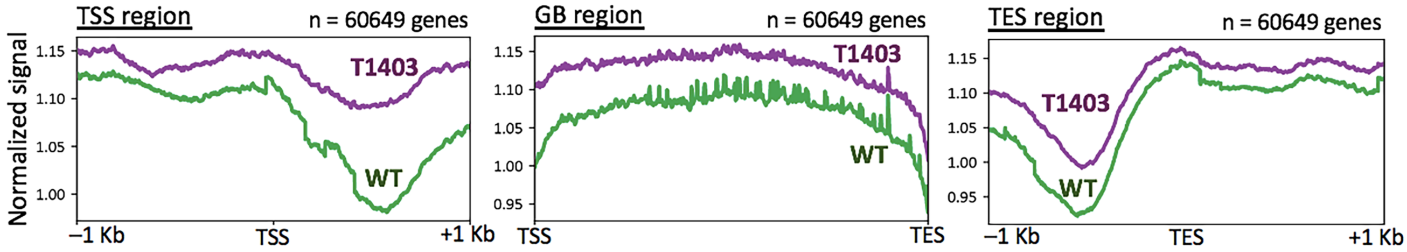

Figure 6-Bunch

Fig. 7.

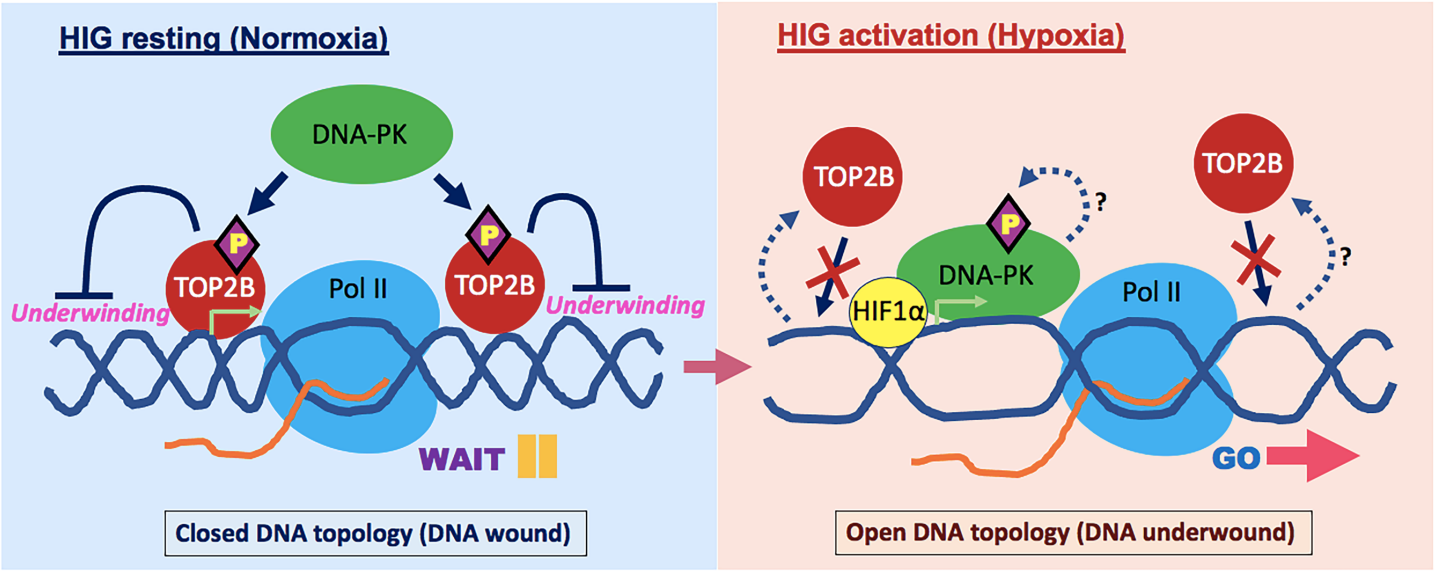

Figure 7-Bunch

Figure Legends

Fig. 1. HIG expression is regulated by TOP2.

(**A**) qRT-PCR results presenting the effect of hypoxic-stress caused by $CoCl_2$ treatment (+$CoCl_2$, throughout the figures) on the transcription of representative HIGs, *p21*, *ALDOC*, and *IL1β*, in SH-SY5Y cells (n= 3 biologically independent samples). An equal amount of H_2O, the solvent for $CoCl_2$, was applied as the control (–$CoCl_2$, throughout the figures). Data are presented as mean values and SD. *P*-values for the bar graphs were calculated with the unpaired, one sided Student's t-test.

(**B**) Representative ChIP-PCR results showing HIF1α and TOP2B occupancies on the representative HIGs, *p21*, *ALDOC*, and *IL1β* under normoxia and hypoxia in SH-SY5Y cells.

(**C**) Representative ChIP-PCR results showing TOP2A occupancy on the representative HIGs, *p21*, *ALDOC*, and *IL1β* under normoxia and hypoxia in SH-SY5Y cells.

(**D**) Representative ICE assay results showing the TOP2A and TOP2B proteins engaged with the chromosomal DNA under normoxia and hypoxia, with or without etoposide treatment (+Eto, 50 μM, 1 h; –Eto, DMSO). Three dots per –$CoCl_2$ or +$CoCl_2$ set are 22, 44, and 66 ng genomic DNA (chromosome) loaded onto nitrocellulose membrane, followed by immunoblotting using TOP2A or TOP2B antibody.

(**E**) qRT-PCR results indicating that under hypoxic stresses, inhibiting TOP2B using etoposide and ICRF193 stimulates transcription at the representative HIGs, *p21*, *ALDOC*, and *IL1β* (n= 3 biologically independent samples). Data are presented as mean values and SEM. *P*-values for the bar graphs were obtained through one-way ANOVA with multiple comparisons.

Fig. 2. DNA-PK modulates TOP2B to suppress representative HIG expression.

(**A**) Immunoprecipitation results showing TOP2B–DNA-PK interaction. INPUT, 0.7% HeLa NE used for each reaction.

(**B**) Immunoblots of DNA-PK, TOP2B, and γH2AX, comparing WT and DNA-PK KO HCT116 cells. ACTIN, a reference.

(**C**) Immunoblots of HIF1α, comparing WT and DNA-PK KO cells. ACTIN, a reference.

(**D**) ChIP-qPCR results showing TOP2B occupancy changes in representative HIGs with or without DNA-PK (n = 3 independent experiments). Data are presented as mean values and SD. *P*-values for the bar graphs were calculated with the unpaired, one sided Student's t-test.
(**E**) qRT-PCR results presenting the effects of DNA-PK KO on representative HIG transcription (n = 3). Data are presented as mean values and SD. *P*-values for the bar graphs were calculated with the unpaired, one sided Student's t-test.

Fig. 3. HIG and a large number of genes are regulated by TOP2B–DNA-PK interaction.
(**A**) Heatmaps illustrating HIG expression analyzed by RNA-seq data. Genes, whose expression is significantly increased (left, n = 192) or decreased (right, n = 66), are shown. $|Log_2FC| > 0.5$, $p < 0.05$.
(**B**) Heatmap presenting differentially expressed genes in the absence of DNA-PK. Upregulated (n = 2706) and downregulated (n = 1994) genes. $|Log_2FC| > 0.5$, $p < 0.05$.
(**C**) Venn diagram displaying the genes that are regulated by hypoxic stress and DNA-PK.
(**D**) Graphs showing mRNA expression of important HIGs in RNA-seq data. Green-purple and green-orange graphs are the representative genes that are downregulated and upregulated in DNA-PK KO cells, respectively. $p < 0.05$.
(**E**) Volcano plot exhibiting the genes that are occupied by TOP2B (red dots in upregulated genes or blue dots in downregulated genes under hypoxic stress).
(**F**) Volcano plot exhibiting the genes that are occupied by TOP2B (red dots in upregulated genes or blue dots in downregulated genes in DNA-PK KO cells).

Fig. 4. TOP2B regulates HIF1α and DNA-PK recruitment and activity in HIGs
(**A**) Immunoblots showing the protein levels of TOP2B and DNA-PK in WT and TOP2B KO SH-SY5Y cells. ACTIN, a reference.
(**B**) ChIP-qPCR results showing DNA-PK occupancies on representative HIGs with or without TOP2B (n = 3 independent experiments). Data are presented as mean values and SD. *P*-values for the bar graphs were calculated with the unpaired, one sided Student's t-test.
(**C**) ChIP-qPCR results showing pDNA-PK occupancies on representative HIGs with or without TOP2B (n = 3 independent experiments). Data are presented as mean values and SD. *P*-values for the bar graphs were calculated with the unpaired, one sided Student's t-test.

(**D**) ChIP-qPCR results showing HIF1α occupancies on representative HIGs with or without TOP2B (n = 3 independent experiments). Data are presented as mean values and SD. *P*-values for the bar graphs were calculated with the unpaired, one sided Student's t-test.
(**E**) qRT-PCR results presenting the effects of TOP2B KO on representative HIG transcription (n = 3 biological samples). Data are presented as mean values and SD. *P*-values for the bar graphs were calculated with the unpaired, one sided Student's t-test.

Fig. 5. TOP2B phosphorylation by DNA-PK is repressive for HIG transcription
(**A**) Primary sequences of representable TOP2B fragments identified by phosphopeptide mass spectrometry. The sequences unique to TOP2B are underlined. The phosphorylatable residues within the unique sequences and mutations generated in this study are in red.
(**B**) Immunoblots of TOP2B and γH2AX. Plasmids expressing WT and mutant TOP2B proteins were transfected into TOP2B KO SH-SY5Y cells. Vec, an empty plasmid as a control. ACTIN, a reference.
(**C**) qRT-PCR results showing the effects of mutant TOP2B proteins on representative HIG transcription (n = 3). Data are presented as mean values and SD. *P*-values for the bar graphs were calculated with the unpaired, one sided Student's t-test.
(**D**) qRT-PCR results showing the effects of T1403A and S1526A TOP2B mutations on representative HIG transcription under hypoxic conditions (n = 3). Data are presented as mean values and SD. *P*-values for the bar graphs were calculated with the unpaired, one sided Student's t-test.

Fig. 6. TOP2B restricts "DNA openness" to prevent HIG activation under normoxia.
(**A**) Schematic representation of TMP-seq sample preparation. TMP, red diamond; cells, yellow circles; DNA, double sky-blue lines.
(**B**) Metagene analyses (left, line graphs) and heat maps (right), comparing underwound genomic regions in WT and TOP2B KO cells. X axis shows distance from TSS or TES in Kilobases.
(**C**) Metagene analyses showing DNA topology changes in HIGs (n = 192) under normoxia (–hypoxia) and hypoxia (+hypoxia) in the WT cells. The genomic region undergoing dramatic DNA unwinding under hypoxia (approximately +200 from TSS) is marked with a red asterisk (approximately +200 from TSS) in a green box.
(**D**) Metagene analyses showing DNA topology changes in HIGs (n = 192) under normoxia (–hypoxia) and hypoxia (+hypoxia) in the TOP2B KO cells. DNA is more underwound under normoxia and the

dramatic DNA unwinding under hypoxia in the WT cells, marked in a green box, is less noticeable in the absence of TOP2B.

(**E**) Chromosome views of a representative HIG, *ALDOC*, comparing the gene locus in the WT (blue peaks, upper) and TOP2B KO (red peaks, lower) cells. TOP2B KO drives open DNA conformation in HIGs.

(**F**) Metagene analyses of all genes (n = 60649) in WT and TOP2B KO cells. Without TOP2B, genomic regions are more underwound under normoxia and proper hypoxia-mediated gene induction is deregulated.

(**G**) Metagene analyses of all genes (n = 60649) in TOP2B KO cells transfected with WT TOP2B (sky-blue line)- or T1403A TOP2B (red line)-expressing plasmids. TOP2B T1403A, a mutation unphosphorylatable by DNA-PK, increases DNA underwinding throughout the promoter, TSS, GB, and TES, in particular at around +600 regions from the TSS, genome-wide.

Fig. 7. A model of TOP2B regulation in HIG transcription.

Under normoxia, TOP2B is associated with HIGs and DNA-PK phosphorylates TOP2B at the CTD including T1403 (phosphorylation marked with a yellow letter “P” in a purple diamond). This phosphorylation is likely to stimulate TOP2B to relax negative DNA supercoiling, preventing DNA underwinding and gene activation. Under hypoxia, TOP2B is released from HIGs by currently unknown mechanisms. Instead, DNA-PK is recruited to HIGs along with HIF1α and is phosphorylated at T2609. Nascent RNA, an orange curved line. TOP2B release and inactivation promote DNA openness/underwinding to facilitate productive Pol II transcription in HIGs. Less defined and characterized processes are shown in dashed lines with question marks. DNA, double blue helical lines; RNA, orange curved lines; TSS, a light green arrow on the DNA.